Imperial College London

Conceptual Design Report

Imperial College London, Department of Aeronautics

Academic responsible: Dr Errikos Levis

Module: Aerospace Vehicle Design

Academic year: 2022/2023

Group: 6

Students: Brice Appenzeller

Ayooluwa Babalola

Benjamin Frisch

Edward Grantham

Antoine Pigamo

Fabienne Rosenblatt

Date: 02/12/2022

Abstract

The following report describes the conceptual design for a short-range/regional jet aircraft operating in New Zealand.

The target design specifications are the following (1):

- **90 passengers + baggage + 2 pilots + 3 cabin crew** to accommodate
- First cruise segment at an altitude of **25,000 ft and Mach 0.69**
- A fourth mission leg (**Diversion**) following a **missed approach**
- Cruise to alternate destination **370 km** away
- Loiter at **5,000 ft for 45 minutes**
- Capable of reaching **Mach 0.75** at cruise altitude
- Absolute ceiling of **40,000 ft** amsl at V_x
- Comply with all **FAR-25** regulations

This conceptual design report follows on from the Poster presentation feedbacks and tackles each part of the design process (1). In this section the baseline configuration of a T tail plane with low wings and aft body mounted engines was made. A NACA 63 015 aerofoil was selected due to it's favourable high lift and super critical characteristics. The parameters of the wings were then set and high lift devices were added to ensure the aircraft could land at all the required airfields especially at Hamilton where landing distance is very constrained. A medium bypass jet was selected to maximise fuel efficiency and sized to match the exact thrust required. The inlet and nozzle dimensions were specified . The tailplane and fuselage were designed and then the important task of conducting a weight and balance analysis of the undercarriage that had been chosen and the systems that had been selected to provide all the necessary function the aircraft requires as well as all the other components on the aircraft. The centre of gravity was found. After this the drag calculations were performed and a stability analysis was performed the aircraft operated well in the flight envelope .

Contents

1 Nomenclature

W_0	Maximum Take Off Weight
Wf	Fuel Weight
We	Empty Weight
L	Lift
D	Drag
S_{ref}	Reference Surface
$S_{flapped}$	High lift devices surface
S	Stroke (Undercarriage)
T	Thrust
W_0/S	Wing Loading
Cl	Lift Coefficient
$Cl\ max, swept$	Maximum Cl with swept wings
$C_{l_{Des}}$	Cl designed
C_{l_α}	Cure lift slope
α_0	Angle which gives C_{l_0}
Cd	Drag Coefficient
e	Oswald efficiency
q	Dynamic pressure
M	Mach number
Mdd	Drag Diversion Mach Number
$M°$	Freestream Mach Number
Vto	Take Off Velocity
Vs	Stall Speed
Va	Approach velocity
Λ_{25}	Quart chord sweep
t/c	Thickness to chord ratio
λ_{opt}	Taper ratio
i_w	Wing incidence
φ_{Hl}	High Lift Devices tilt
$P1$	Pressure at the engine
$P0$	Atmospheric pressure

BPR	Bypass Ratio
SFC	Specific Fuel Consumption
Sv	Vertical stabiliser aera
Sh	Horizontal stabiliser aera
$Wi\ max$	Maximum width (Fuselage design)
$H\ max$	Maximum Height (Fuselage design)
D_f	Fuselage diameter
L_{nose}	Nose Length
L_{cabin}	Cabin Length
$L_{afterbody}$	After Body Length
APU	Auxiliary Power Unit
IDG	Integrated Drive Generator
GPU	Ground Power Unit
RAT	Ram Air Turbine
TODA	Take Off Distance Available
LDA	Landing Distance Available
PCN	Pavement Classification Number
ACN	Aircraft Classification Number
V_v	Touch down sink speed
N_g	Gear Load Factor
η	Shock absorber efficiency
η_T	Tire efficiency
x_{CG}	x position of the centre of gravity
z_{CG}	z position of the centre of gravity
$\alpha_{0,w,clean}$	zero lift angle of attack
$C_{f,c}$	Skin friction coefficient
FF_c	Form factor
Q_c	Interference factor
$\frac{S_{wet,c}}{S_{ref}}$	Wetted area ratio
$C_{D,misc}$	Miscellaneous drag coefficient
$C_{D,L+P}$	Leakages and protuberances drag coefficient

λ_F Length of fuselage divided by its diameter

Λ_m Sweep maximum thickness

CD_π Drag of miscellaneous components

C_{D_i} Induced Drag

Λ_{LE} Sweep of the leading edge

C_{m_α} Moment coefficient

S_G Ground roll distance (performance)

μ Friction coefficient (performance)

S_R Rotation distance (performance)

S_{CL} Climb distance (performance)

γ_{CL} Angle of climb

h_{OBS} Obstacle height

S_{TR} Transition Distance (performance)

D_{AOE} Drag of the aircraft with all the engines operative

S_a Approach distance (performance)

γ_a Descent gradient

S_F Flare distance (performance)

S_{FR} Touchdown distance (performance)

S_B Braking distance (performance)

P_S Excess Specific Power

2 Introduction

This report aims to detail the conceptual design and discuss the quality of the resulting design. The conceptual design focuses on the initial sizing process, including the design of the baseline configuration and the weight as well as wing and thrust sizing, and the selection choices in high lift devices.

2.1 Baseline Configuration

2.1.1 Wings

Low-mounted wings are used to ensure uncomplicated maintenance and refuelling during turnovers at airports, which also has an economic benefit since it is easier to access the engines and quicker to refuel. Furthermore, they offer structural benefits which affect the passengers' safety in a positive way: The wing does not pass through the cabin, which prevents the passengers from falling over it and presents the opportunity of board service. In the event of water landing, the fuselage is kept above water and even in the event of a crash, low mounted wings absorb more energy than high mounted wings. Despite the advantages of low mounted wings, they experience more ground effect during landing than high mounted wings. Plus, they do not offer much ground clearance, which needs to be considered when choosing engines under the wing; to avoid this issue fuselage-mounted engines have been chosen, as stated in the following.

2.1.2 Engines

The two aft-fuselage-mounted engines lower the risk of foreign object damage as well as friction drag due to the lower overall surface area. They offer a good crosswind landing capability, which is important considering the given and determined mission profile and target design specifications, because New Zealand is one of the windiest countries in the world. Even in the case of OEI, the engines provide less asymmetric thrust since the engines are closer to the centre line. However, there are disadvantages regarding the maintenance, which is difficult, expensive and time consuming, and the fuelling because the engines are located further from and above the fuel in the wings so that more piping and a more powerful and therefore heavier fuel pump are needed. Additionally, due to the position of the engines, attention should be drawn to engine stall and surge at high angles of attack. Fuselage-mounted engines also produce more noise inside the cabin, what is disturbing for the passengers.

2.1.3 Tail

The selection of aft-mounted engines leads to a t-tail being designed. The t-tail provides aerodynamic advantages: The control during spinning is better, it reduces the effects of vortices from the rudder and effects of the wing's downwash are being reduced by the high-mounted elevator. The disadvantages are similar to those of the aft-mounted engines as the t-tail is harder to install and maintain, heavier than a conventional tail and more susceptible to deep stall.

2.1.4 Undercarriage

Given the fact that the aircraft is designed to have low mounted wings, these accommodate wing undercarriage mounting, which opens the opportunity of applying a tricycle undercarriage. This supports the crosswind landing capability of the engines, and the ground handling as there occurs no ground loop. A tricycle undercarriage makes loading and unloading easier as the fuselage is horizontal when landed (as a contrast to taildragger landing gear) which also leads to better visibility during taxi, take-off and landing. Nevertheless, landing on unpaved surfaces risks damage to the front gear and it is prone to breaking. A tricycle undercarriage is heavier than other configurations and susceptible to tail strikes.

2.2 Initial Sizing

2.2.1 Initial weight sizing

This initial weight sizing work aims to determine values such as W_0, W_e, W_f and the following weight fractions: $\frac{W_e}{W_0}$ & $\frac{W_f}{W_0}$. These values are obtained using empirical equations and physical assumptions such as:

- The Breguet range and endurance equations (2).
- Selection of SFC and lift to drag ratio $\frac{L}{D}$ (3)
- Selection of weight fractions for warm-up, taxi, take-off, climb, descent, and landing in literature (3)

By using these results, the weight sizing final values are:

W_0	W_e	$\frac{W_e}{W_0}$	W_f	$\frac{W_f}{W_0}$
48790 kg	24763 kg	0.51	14887 kg	0.31

Table 2-1 Weight sizing values

2.2.2 Initial wing and thrust sizing

The second part of the initial sizing considers every constraint that the aircraft must confront at each stage of this 4 legs mission (3 cruise segments and a missed approach). Every constraint is visualized in a graphic called the constraint diagram gathering every thrust to weight ratio denoted $\frac{T}{W_0}$, and every wing loading $\frac{W_0}{S}$ for each leg. This diagram defines a feasible zone for our design and allows to choose for an optimal design based on a trade-off between thrust to weight ratio and wing loading. This leads to the following diagram with the optimal design point selected:

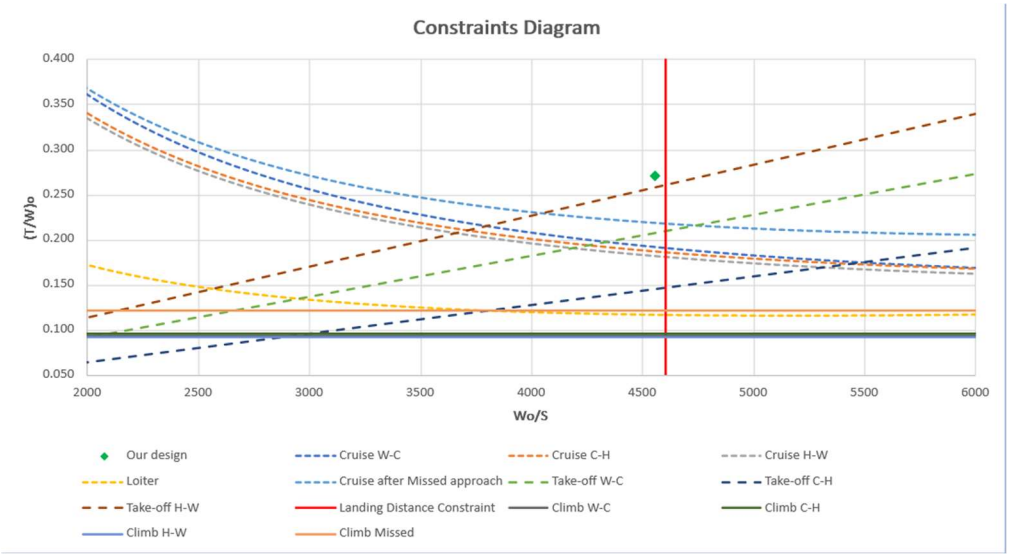

Figure 2-11 Constraint diagrams and design point

The selection of the optimal point is made by assuming a minimization of the thrust to weight ratio and maximization of the wing loading. As a matter of fact, the limit of the engine is not reached during cruise. The detailed placement of the design point also considers a security structure factor, thus reducing slightly the wing loading value compared to the landing distance constraint.

Finally, the design point leads to the initial sizing final values:

$\frac{T}{W_0}$	$\frac{W_0}{S}$	T_0	S
0.270	4556 N/m^2	129.44 kN	105.06 m^2

Table 2-2 Initial sizing final values

3 Aerofoil Selection

3.1 Design Lift Coefficient

To evaluate the many characteristics of different aerofoils, sufficient appropriate data is required. Specifically experimental data is required as programs (such as XFOIL) which attempt to calculate similar data are accurate only within the linear range of a lift curve slope and below 0.4 Mach (4). This narrowed down the selection of aerofoils considered to NACA aerofoils.

The primary consideration in the selection of an aerofoil was the lift to drag ratio at the design lift coefficient. This was considered as one of the most important attributes due to the design's brief of a commercial aircraft. Maximizing the lift to drag ratio for constant lift minimizes drag therefore lowering costs, the most important concern of a commercial

aircraft. The design lift coefficient is set to be the lift coefficient at cruise as this is the condition at which the aircraft will spend most time and will therefore benefit from the drag reductions. The cruise and therefore design lift coefficient is given in equation (*5.1*) where q is the dynamic pressure and the wing loading is the value chosen in initial sizing. This yields a value of $C_{l_{Des}}$ =0.363432.

$$C_{l_{Des}} = \frac{1}{q}\left(\frac{W}{S}\right) \tag{5.1}$$

The experimental data used was recorded at below Mach 0.3. Compressibility affects therefore needed to be accounted for. This was done by multiplying the design lift coefficient which is the in the compressible range by the Prandtle-Glauert compressibility factor as seen in equation (5.2) to find the corresponding incompressible lift coefficient. The corresponding value for the coefficient of drag at that lift coefficient was then divided by the compressibility factor to give the compressible coefficient of drag as seen in equation (5.3). The experimental data used however has data for Reynolds numbers only up to $9*10^6$ which is noticeably different to the Reynolds number at the cruise which range from $2.75*10^7$- $2.87*10^7$his will likely result in the experimental results having a lower lift to drag ratio.

$$C^*_l = \sqrt{1-M^2} * C_l \qquad (5.2) \qquad\qquad C_D = \frac{C^*_D}{\sqrt{1-M^2}} \qquad (5.3)$$

3.2 Thickness to chord ratio

To narrow down the amount of aerofoils considered, the typical range thickness to chord ratio (t/c) of similar aircraft namely regional jet transports was found to be 10- 13% thickness to chord ratio. Due to this design's baseline configuration not having wing mounted engines (which would act against wing loading caused by creating lift), the structural weight of the wing is anticipated to be larger than normal. As the mass of a wing is approximately inversely proportional to the square root of the thickness to chord ratio, it was decided to consider a thickness to chord ratio range above the similar aircraft range (which mainly had wing mounted engines) . Specifically, aerofoils between 12-15% thickness ratios were considered.

3.3 Maximum Lift Coefficient

Another major characteristic considered was the aerofoil's maximum lift coefficient. This is a specifically important attribute due to the high estimate of a $C_{l_{max}} = 3$ from initial sizing. The higher the maximum lift coefficient of the aerofoil, the higher the maximum lift coefficient of the clean wing will be. This decreasing the required increase in maximum lift coefficient due to the high lift devices which allows for less complex high lift devices, therefore saving cost, as well as a decrease in the drag caused by flaps as a lesser deflection angle is required.

3.4 Critical/Drag Divergence Mach Number and Quarter Chord Sweep (Λ_{25})

The final major factor considered when evaluating aerofoils is the critical and drag divergence Mach number. Critical Mach number is the minimum free stream Mach number at which flow over the wing becomes supersonic. Above the critical Mach, flow over some part of the aerofoil is supersonic therefore a shock is produced which leads to the separation of the boundary layer and an increase in drag.

The drag divergence Mach number M_{DD} is defined as the Mach number at which there is an increase in wave drag of 0.002. The drag divergence Mach number of an aerofoil can be calculated using equation (5.4) where K_A = 0.87 for 6 series NACA aerofoils (the only options shortlisted) (5).

$$M_{DD} + \frac{C_{l_{Des}}}{10} + \left(\frac{t}{c}\right) = K_A \tag{5.4}$$

Sweeping a wing, results in a smaller component of the flow's velocity being perpendicular to the wing . Therefore, the amount of sweep is set in order to reduce the effective Mach number perpendicular to the wing, to be equal to the highest mission Mach number of 0.716. This gives the relationship in equation 5.5 with x=1 .

$$\Lambda_{25} = \cos^{-1}\left(\frac{M_{DD}}{M_\circ}\right)^x \tag{5.5}$$

In practice however the sweep predicted by this relationship was found to not be sufficient in reducing the effective Mach number enough, therefore an empirically determined exponent of 0.5 is introduced which was used to calculate the necessary sweep angles for all aerofoils. A higher sweep angle is unfavourable as it leads to increased induced drag and lower lift coefficients. The swept max lift coefficient has therefore been calculated using equation 5.6 to best analyse each aerofoil's performance. The sweep of the wing also notably reduces the increase in maximum lift coefficient due to high lift devices in the same relationship as seen later in this report in equation (5.6).

$$C_{l_{max,Swept}} = \cos \Lambda_{25} C_{l,max} \tag{5.6}$$

Due to this design configuration having a T tail, there is an additional constraint on sweep. Namely that a T tail requires the wing to not have poor wing alone pitch up characteristics in the event of stall. This phenomenon is affected by aspect ratio and sweep, the boundaries for which can be seen in figure 5-1. To maintain the previously determined aspect ratio, sweep must be less than approximately 13°. A higher sweep would be possible but would necessitate a lower aspect ratio, which currently at 8.5 is fairly low for a jet transport, which would result in higher induced drag. This constraint also provided the upper range on possible thickness to chord ratios as a higher ratio would require too much sweep.

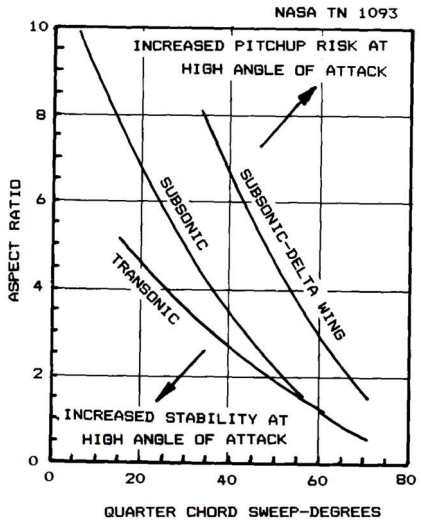

Figure 3-1 Pitch up Seep and aspect ratio Boundaries (6)

3.5 Aerofoil selection and Stall characteristics

In order to evaluate these aerofoils, a normalized merit index (m) was created including the major four attributes discussed. Notably due to the initial sizing's high maximum lift coefficient and the baseline configuration's heavier wings due to lack of wing mounted engines, the maximum lift coefficient and thickness to chord ratio terms were given a 20% larger weighting in the merit index. Aerofoils with a merit index above 0.9 were shortlisted in table 5-1. A description of each aerofoils stall characteristics is also provided.

Name	L/D	$\frac{1}{\sqrt{t/c}}$	$C_{l_{max,swept}}$	Λ_{25}	MI	Stall Characteristics
NACA 631212	56.6	2.89	1.613	5.39	0.921	Stable, Quite abrupt
NACA 631412	50.5	2.89	1.752	5.39	0.924	Stable, Slightly abrupt
NACA 641112	58.6	2.89	1.493	5.39	0.908	Stable, Gradual
NACA 641212	60.6	2.89	1.573	5.39	0.927	Stable, Slightly abrupt
NACA 641412	56.0	2.89	1.643	5.39	0.924	Stable, Gradual
NACA 651212	68.7	2.89	1.444	5.39	0.931	Stable, Quite Abrupt
NACA 651412	67.8	2.89	1.673	5.39	0.964	Stable, Gradual at high Reynolds number, Slightly abrupt for lower Reynolds numbers

NACA 661212	73.6	2.89	1.468	5.39	0.949	Stable,Very abrupt
NACA 661415	69.6	2.58	1.564	12.98	0.923	Stable, Quite gradual

Table 3-1 Summary of aerofoils characteristics

From the information in table 5-1 the NACA 65_1412 aerofoil was chosen as it has the 4th highest lift to drag ratio, the 2nd highest swept maximum lift coefficient, has the tied lowest sweep amount which overall yields the highest merit index. The only downsides of this aerofoil is that it is not the lightest as it has a low thickness to chord ratio and at low Reynolds numbers the stall characteristics are slightly abrupt This is a reasonable trade-off firstly as take-off and landing occur at a Reynolds number of $1.16*10^7$ and $1.36*10^7$ (velocity at take-off and landing found using equation 5.7,5.8 and 5.9)well above the slightly abrupt stall experimental data. Secondly, as this design is for a commercial aircraft, professional pilots will be more than able to handle the slightly less than ideal stall characteristics especially due to the inclusion of a stick shaker and wing twist as discussed later in the report.

$$V_S = \sqrt{\frac{2\left(\frac{W}{S}\right)}{\rho C_{l_{max}}}} \quad (5.7) \qquad V_{TO} = 1.1V_S \quad (5.8) \qquad V_A = 1.2V_S \quad (5.9)$$

4 Wing Design

4.1 Twist

One purpose of wing twist is to ensure that the tips of the wings stall after the root, this results in even a poorly stalling aerofoil having a gradual stall (6). In order to achieve reasonable stall characteristics, twist is usually set at -3°. Twist also contributes to producing an elliptical lift distribution which will be discussed later but provides the lower limit on twist at -5° as beyond which lift to drag ratio reduces at lift coefficients other than $C_{l_{Des}}$ (6). As the stall characteristics of the aerofoil are not to undesirable, a geometric twist of -3° is chosen as geometric twist makes analysis easier and therefore more accurate.

4.2 Taper Ratio

Minimum induced drag is achieved when the lift distribution is elliptical. Taper ratio along with twist and sweep are three major factors that effect a wing's lift distribution. Equation 6.1 gives an approximation for the ideal taper ratio needed for a given sweep (given in degrees). This yields an initial value of 0.399.

$$\lambda_{opt} = 0.45e^{-0.036\Lambda_{25}} \quad (6.1)$$

As previously mentioned, the twist of a wing also affects the lift distribution. Specifically, it results in a higher taper ratio in order to produce an elliptical lift distribution than initially predicted. Therefore, a value of 0.471 was chosen based on a 18% increase according to historical data (6). A value of 0.471 is a reasonable as it provides sufficient areas near the tip of the wing for ailerons as well as avoiding unfavourable tip stall characteristics. A lower taper ratio also results in a larger chord at the root of the wing, which is better in a structural sense, provides greater volume for this design's wing located retractable undercarriage and results in a greater proportion of the wings aera being closer to the root where flaps are typically located, therefore increasing their effect on the maximum lift coefficient.

4.3 Dihedral

The Purpose of dihedral is to provide stability along the longitudinal axis. (7) his is caused by a sideslip during a bank which results in an increase in angle of attack of the lowering wing therefore returning it to stable flight. This returning pitching moment is proportional to the dihedral angle. A high dihedral angle improves stability in the spiral mode but too high results in an unstable Dutch roll. Other factors provide effective dihedral such as wing location and amount of sweep. From literature, a typical dihedral range for a low mounted upswept wing is 5-7° while for a swept low wing the range is 3-7°. This decrease in the lower bound is due to the effective dihedral caused by increased sweep with approximately every 10° of sweep yielding 1° of effective dihedral. Applying this to this design's fairly low sweep yields a design specific range of 4.45-7°. A dihedral angle on the lower end of the range of 5.25° was chosen. This value was chosen as it results in the undercarriage being closer to the ground therefore making it smaller and as this design's baseline configuration not having wing mounted engines means there is less need for ground clearance caused by the

dihedral angle. It is also typical for aircraft design to prioritize Dutch roll stability over spiral stability (8), further justifying the choice.

4.4 Wing Incidence (i_w)

The two factors defining the optimal incidence angle is reducing the drag of the fuselage and having a horizontal cabin during cruise conditions. These two conditions both require that during cruise conditions the fuselage is parallel to the freestream. For the fuselage to be horizontal during cruise conditions the incidence angle is be given by the equation (6.2) where C_{l_α} is the lift curve slope of the wing (as calculated later in the report)

$$i_w = \frac{C_{l_{Des}}}{C_{l_\alpha}} + \alpha_0 \tag{6.2}$$

As the expression for incidence angle is a function of Mach number, there are different optimal incidence angles for the different Mach number cruise segments. As incidence angle is a fixed quantity, the lowest calculated incidence angle of was initially taken. This is chosen because during non-optimal cruise segments where a higher angle is required, the fuselage will have a positive angle of attack. This is superior to taking the maximum incidence angle as for such an angle, during non-optimal cruise segments the fuselage would have a negative angle of attack therefore producing negative lift and increasing overall drag. This value was then reduced by 0.4° in order to allow for a possible pitch down of the aircraft once the lift of the horizontal tail plane is considered for stability reasons. Thus giving an incidence angle of 4.03°

4.5 Wing Tip Devices

In initial sizing it was decided to have an aspect ratio, on the lower end of the typical range for a jet transport in order to reduce the weight of the wing which was assumed to be high due to not having wing mounted engines. The major downside of a low aspect ratio is an increase in induced drag due to tip vortices. To reduce this affect, it was decided to have wing tip devices, which reduce induced drag by acting as a wall between the high- and low-pressure air which reduces the strength of wingtip vortices. (9) Specifically, winglets, a wing tip device which generates a lift force with a forward component to act in the opposite direction of drag were chosen. Winglets were chosen as they provide the largest reduction in induced drag for low aspect ratio wings such as this design, due to the stronger wing tip vortices. A typical winglet geometry can be seen in figure 6-1. The downsides of winglets include an increased wetted area, worse flutter tendencies and potential ground clearance issues which provide bounds for the winglet dimensions. With regards to ground clearance, this design's configuration aims to have a low fuselage and therefore wing to meet the design specification of a fast turnaround time. It was therefore decided to not have a lower winglet in order to avoid possible ground clearance issues as the lower winglet contributes less to the drag reduction. The practical effect of winglets is that they increase the wings effective aspect ratio beyond its physical dimensions. From similar aircraft a height (a) of 2m was which gives a value of $2\frac{a}{b} = 0134$. Not having a lower winglet yields a value for $\frac{a}{c} = 0.875$, therefore yielding a value for $(1 - \delta_E)$ of 0.875 which according to equation 6.3 (7) gives an effective aspect ratio of 9.71. This 11.4% increase in effective aspect ratio is within the 20% range rough estimate from literature (6) and is therefore an appropriate value.

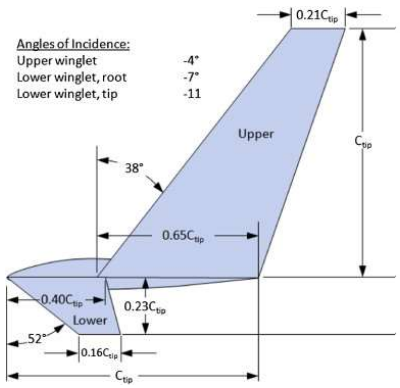

Figure 6-1 (10)

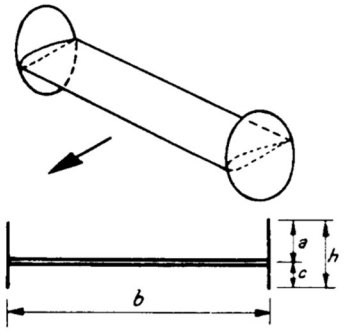

Figure 6-2 (7)

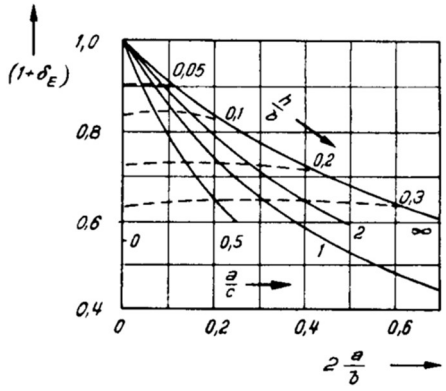

Figure 6-3 (7)

$$A_{eff} = \frac{A}{(1+\delta_E)} \tag{6.3}$$

5 High Lift Devices and Control Surfaces

5.1 $\Delta C_{L_{max}}$

The purpose of high lift devices is to increase the maximum lift coefficient at take-off and landing conditions (This analysis, will focus on landing conditions and then multiply by 0.8 for take-off). The total maximum lift coefficient is given by equation 7.1 as the sum of the maximum lift coefficient of the clean wing and the change in maximum lift coefficient due to the high lift devices.

$$C_{l_{max}} = C_{l_{max,clean}} + \Delta C_{L_{max}} \tag{7.1}$$

$C_{l_{max,clean}}$ can be calculated from the aerofoil's sectional maximum lift coefficient using equation 7.2which accounts for 3D effects as well as sweep. The value obtained is $C_{l_{max,clean}}$=1.505. As the total $C_{l_{max}}$ has been previously chosen to be $C_{l_{max}}$ =3 in initial sizing, The total coefficient of lift contribution of the high lift devices ($\Delta C_{l_{max}}$) was found to be 1.495.

$$C_{l_{max,clean}} = 0.9\, C^*{}_{l_{max,clean}} \cos\varphi_{25} \tag{7.2}$$

To reach this value of $\Delta C_{l_{max}}$, there are a variety of options, falling into the category of either leading or trailing edge devices. From an analysis of similar aircraft, a combination of both leading and trailing edge devices was deemed appropriate with an initial prediction of slats and double slotted flaps in initial sizing. The $\Delta C_{L_{max}}$ contribution of each type of high lift device was however considered as given by equation 7.3 where $\Delta C_{l_{max}}$ is given for multiple high lift devices in appendix I. The chord ratios (c'/c) are discussed in a later section.

$$\Delta C_{L_{max}} = 0.9 \Delta C_{l_{max}} \left(\frac{S_{flapped}}{S_{ref}}\right) \cos\varphi_{HL} \tag{7.3}$$

5.2 High Lift device and Aileron Sizing

The ratio $\frac{S_{flapped}}{S_{ref}}$ is defined as seen in figure 7-1. To maximize $\Delta C_{L_{max}}$, this ratio is ideally maximized by having high lift devices on as much of the span as possible. Other components however take up parts of the span, namely, the fuselage, ailerons, winglets and gaps between components. The leading edge notably only has the fuselage, winglets and leading-edge devices as ailerons are only located on the trailing edge.

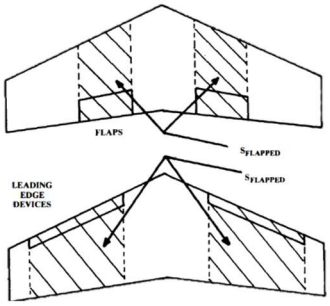

Figure 5-1 Geometry drawing of high lift devices

As the geometry of the fuselage has already been determined, it's percent span can be determined as the ratio of its width to the wingspan resulting in a span between 0-10.8%. It is important to have leading edge devices along the majority of a wing's span to increase its effect on maximum lift coefficient and as one effect of leading-edge devices is the increase in the stall angle. Therefore, if a portion of the wing is not covered by leading edge devices, it will stall at a different angle of attack to the rest of the wing which is undesirable. Therefore, the leading-edge devices are located from 10.8-97.2%, leaving a 1% gap between the aileron and the winglets which have a % span of 0.88% as the geometry is already known. The percent span of flaps is also ideally as high as possible therefore will span from 10.8% all the way to the span location of the ailerons. Ailerons are located as near as possible to the wing tips in order to increase their moment arm, however due to wingtip vortices, any increase in aileron span beyond 90% has little benefit. Therefore, the ailerons will end at a span of 90%. The typical percentage span of ailerons is given by literature to be in the range of 20 to 30% from historical data. As the required maximum lift coefficient is fairly high, a value of 20% is taken resulting in an aileron span between 70-90%. This provides the upper bound for the span of the flaps giving a span between 10.8-69% with a 1% gap between the flaps and ailerons. Finally, the 10% span between the ailerons and wing tip provide sufficient space for the winglets which have a percentage span of only 0.88%. The %span ranges of all components is given in table 7-1.

Component	Span Start (%)	Span End (%)	Total % Span
Fuselage	0	10.8	10.8
Leading Edge Devices	10.8	97.2	86.4
Flaps	10.8	69	58.2
Ailerons	70	90	20
Winglets	98.2	100	1.8

Table 5-1 Span start and end as a percentage of the characteristic length for different components

5.3 Additional Control Surfaces

To account for being on the low end of aileron span% range, the percent chord ratio is taken to be at 30%, the highest possible value within the constraints of the spar location and actuation mechanism sizing. Spoilers however will also be used to aid in roll control. A spoiler consists of a hinged plate which when raised, spoils the airflow over that part of the wing resulting in an imbalance of lift causing the aircraft to roll. Another benefit of spoilers is that it allows for control of the aircraft in the case of aileron reversal, a phenomenon where a aileron deflection results in a roll movement contrary to what is intended. This occurs at high dynamic pressure and can be resolved by having spoilers on the inboard section of the wing notably in the span of the flaps. The spoiler mechanism (along with the flap actuation) is assumed to require 4% based on a similar mechanism (7). This spacing provides the most limiting constraint in terms of chord percentage therefore defining the aftmost location of the rear spar. This also therefore sets the maximum chord ratio (c'/c) of the flaps to be 1.29. These values are summarized in table 7-2 and visualized in figure 7-1:

The total chord percentage of the spoiler is taken to be 16% while the span is taken to be 20%, on the high end for similar aircraft. The spoilers are located at a span 5% less than the ailerons such that they can operate in the case of aileron reversal while still maximizing their moment arm (11).

In order to utilize spoilers, a manual flight system cannot be used as they have a non-linear response. This however is not a large imposition as a fly by wire system is most common for similar aircraft as is explored later in section 11.

Component	Chord Start (%)	Chord End (%)	% Chord/(c'/c)
Slat	0	10	(c'/c)=1.1
Flap	72	100	(c'/c)=1.28
Aileron	70	100	% Chord=30
Rudder	1	90	% Chord=30
Elevator	1	90	% Chord=25

Table 5-2 %Chord for different component

The sizing of elevators and rudders is far less constrained by spanwise space and due to this design's t tail configuration, the rudder remains unblanketed as it is out of the wake of the horizontal tailplane. The rudder span was therefore chosen to be from 1- 90% The sizing of the rudder is defined by the case of one engine inoperative which results in a yawing moment which the rudder must be able to account for. This designs configuration of rear mounted engines results in a smaller moment arm and therefore a lower yawing moment. A chord percentage of 30% which is on the low end according to literature was therefore chosen. A typical chord percent range for elevators Like the rudders, the spanwise percentage of the elevators was chosen to be from1-90% with a chord percentage of 25% taken from literature.

The hinge line of all control surfaces was placed at 15% of the chord, therefore shifting the control surfaces centre of gravity forward of the hinge line which reduces flutter tendencies (6).

5.4 High Lift Device Combinations

Using values for %chord and span as well as taper ratio $\frac{S_{flapped}}{S_{ref}}$ was found to have a value of 0.85 for the leading edge devices and 0.62 for the trailing edge devices. Equation 7.3 was then used to find the $\Delta C_{L_{max}}$ of all the listed high lift devices, the various combination which satisfied the needed increase in maximum lift coefficient are seen in table 7-3.

Flaps/Leading edge Devices	**Fixed Slot**	**Leading edge flap**	**Kruger Flap**	**Slat**
Double Slotted	/	/	/	1.501
Triple Slotted	1.537	1.613	1.613	1.720

Table 5-3 Total change in lift coefficient for viable each HLD combination

5.5 Cost Analysis

As there are multiple combinations that at meet the necessary increase in maximum lift coefficient, the final choice is based on finding the most cost effective of these combinations. An estimate for manufacturing cost of a high lift device is given in equation 7.4 (11) where studies have found n empirically to be 0.7. Dividing by the constant and normalizing gives a non-dimensional estimate for the upfront manufacturing cost as a function of mass and part count of the high lift device, as taken from an analysis of similar aircraft (11). The other major cost concern is the maintenance costs of maintaining the different high lift device combinations. For this a index was created by normalizing the complexity term (Part count^n) from equation 7.4 . This assumes that maintenance costs are proportional to the part count as larger part counts suggests more complicated mechanisms therefore requiring more repairs and inspections by better qualified staff. All these considerations result in higher ongoing maintenance costs. Due to availability of data, fixed slot and leading-edge flaps could not be considered, however from an analysis of similar aircraft, they are uncommon.

$$Manufacturing\ Cost = Constant * Mass * (Part\ Count)^n \quad (7.4)$$

This analysis appears to show that a combination of double slotted flaps and slats is the optimal combination for both the manufacturing and maintenance cost indices. Therefore, a combination of slats and double slotted flaps was chosen which yields a maximum lift coefficient of $C_{l_{max,L}}$= 3.01 at landing conditions and a value of $C_{l_{max,TO}}$= 2.41 at take-off, meeting the initial requirements outlined in initial sizing.

6 Powerplant Selection Installation and Integration

6.1 Powerplant Selection

There are several different powerplants available to provide the thrust, bleed air and electrical power required for the aircraft. The powerplant selection was focused to jet engines as this was set in the brief for the aircraft. Within the family of jet engines centrifugal turbojet engines, axial turbojet engines and turbofan engines were all possible powerplants.

When choosing the type of powerplant to use the fuel efficiency and weight were prioritised. This is due to a low fuel efficiency increasing the weight of the fuel we would need to carry and due to the engines being mounted on the aft-fuselage, heavier engines would require a lot of extra structural weight to mount them. In addition to these heavier rear mounted engines will move the centre of gravity towards the tail requiring a larger and heavier tailplane to provide sufficient control.

Out the choices of jet engines high bypass turbo fan engines provide the best fuel efficiency while being operable between Mach 0 – 0.75 where the aircraft will operate between. Both axial turbojets and turbofans are more efficient than centrifugal turbojets and have a smaller frontal area reducing the drag of the powerplant. In contrast to this a turbo jet or low bypass turbofan engine will be lighter than a comparative high bypass turbofan. It was decided a light medium bypass engine would be a good compromise between the requirement of low weight and fuel efficiency.

The engines could be podded or integrated into the fuselage structure however for a fast turnaround design, podded engines are more appropriate as they allow better accessibility for faster maintenance in case of a fault in the engine as well as the replacement of the engines with better more efficient models in the future. The engines can also be removed with less difficulty for inspection. A subsonic pitot inlet provides the best pressure recovery around M = 0.7 for the engine (6) compared to other subsonic inlets such as the NACA inlet allowing a more efficient compression of the incoming flow. Theoretically the pitot inlet provides a perfect pressure recovery.

6.2 Thrust Requirements

The thrust required for the aircraft was determined by the initial sizing. $T_{needed\ per\ engine} = 14550$ lbs or 64.72 kN. This thrust would need to be produced by the installed engine hence the installation losses were approximated for the engine. Due to the engine being mounted close to the fuselage inlet losses for the engine were approximated along with bleed air losses and power extraction thrust loss due to the pressurization and system power requirements respectively. To correct for inlet pressure losses a correction factor was applied to the total pressure loss between the free stream and the engine of 0.98 this is an estimate based on our aircraft having aerodynamic components in front of the fuselage engines. This was applied in equation (8.1) with an ideal pressure recovery of 1 a correction for ram effect of 1.35 typical of a pitot inlet (6).

$$\%Thrust\ lost = C_{ram}\left[\frac{P_1}{P_0}ref - \frac{P_1}{P_0}actual\right] \times 100 \qquad (8.1)$$

The thrust loss due to bleed was calculated using our engine bleed mass flow to total engine mass flow estimated to be 3% to be sufficient, it is towards the upper end of bleed air extraction percentage due to our hydraulic and cabin pressurisation. This was multiplied by a correction factor of 2 accounting for the scaling factor of bleed air on thrust loss given in (6) and the percentage thrust lost was calculated at 6%. The thrust loss due to power was calculated by taking the power extraction per engine at 37500W and divided by cruising velocity to calculate the thrust lost at 169.5N coming to 0.26% of total required thrust. The correction factors used are specified below.

Inlet Pressure Thrust Loss	Bleed Air Thrust Loss	Power Extraction Thrust Loss	Total Thrust Loss
2.7%	6.0%	0.26%	8.96%

Table 6-1 - Installed Engine Thrust Losses

Accounting for these installation losses the new required thrust is 71.5kN.

6.3 Engine Selection and Sizing

Knowing this value, an existing engine was found that produces ±10% of our required thrust. This engine could then be scaled to estimate the dimensions of the aircraft's engines. The General Electric CF34-10E2A1 was found to be suitable the dimensions of the engine are specified in the EASA certification (12) and include thrust reversers and all required accessories listed in appendix F removing the need to adjust the engine weight and diameter to account for these separately. The dimensions are as followed

Engine	Max Thrust [kg]	BPR	Dry Weight inc accessories [kg]	SFC [kg/min]	Max Diameter [m]	Fan Diameter [m]	Length [m]
General Electric CF34-10E2A1	75.44	5.4	2151.73	18	1.86	1.35	4.52

Table 6-2 Real engine chosen to be re-sized with the thrust of the aircraft

It is now necessary to resize the engine for the thrust we really need. A sizing factor can be determined by the ratio of our maximum necessary thrust to the maximum thrust of the engine used with the sensible scaling equations specified in the lecture slides (2).

$$Sizing\ factor = \frac{T_{Needed}}{T_{Engine}} = 0.94 \qquad (8.2)$$

So final values for the engine are:

Scaled length [m]	Scaled Fan Diameter [m]	Scaled Max Diameter [m]	Scaled total weight without nacelle [kg]
4.41	1.31	1.81	2014.69

Table 8-3

6.4 Inlet and Nozzle Design

An important parameter of the inlet is the inlet area, the inlet area should be sized to the capture area so the engine can capture and slow the exact amount of air it will need without spillage or too little air being provided. In addition to this for a subsonic jet the capture area of the inlet should be less that the diameter of the engine fan so the air is slowed between the inlet and the fan. A simple method for calculating the capture area is multiplying the mass flow rate of the engine found in (13) and multiplying it by 0.025sqft lbs^{-1} s^{-1} which is the capture area to mass flow rate ratio taken from a statistical graph in (2) which is a constant for our flight regime giving the inlet capture area of $0.88m^2$. This gives an inlet diameter of 1.06m. Another important parameter are the inner and outer lip radii of the inlet. The engine will need to take air from a large area flowing from around the lips of the engine at take-off and a much smaller area around the centre of the engine at cruise and thick nacelle lips will accommodate for both these cases. Recommendations from Raymer (6) for thick nacelle lips were used to size this and the inner and outer lip radii were set to 0.04m and 0.02m giving a 0.06m thick nacelle lip.

The manufacturer designated fixed converging nozzle was chosen for our engine. The converging nozzle will accelerate the engine exhaust gasses to provide thrust. The optimal nozzle exit mass flow rate can be optimized for each leg of the mission however variable convergent nozzles that will provide the variable nozzle convergence needed for this would come with a weight penalty that far outweighs the improved performance.

6.5 Engine Placement

With the choice of engine mounting on the fuselage various compromises had to be made to achieve an optimum placement. The weight of the engines mean that extra structures will be needed to reinforce the rear fuselage and the further away the engines are placed from the fuselage the heavier the pylons connecting the engines to the fuselage will be. Placing them as close to the fuselage as possible will reduce this weight but also come with an increased drag due to interference between the fuselage and the engines which can be as high as 60 – 80% (14). It was decided to place the

engines directly adjacent to the fuselage and pay this drag penalty due to the significant weight of the engines. The effects of the fuselage boundary layer were considered and the distance from the engine maximum radius where the engines will be mounted, to the inlet radius is 0.25m large enough that the fuselage boundary layer should not affect the flow into the engine inlet. Finally, the engines were mounted canted upwards by 3° to account for downwash from the wing as well as the slight angle of attack we will be flying at during cruise as well as a 1° nose out cant due to flow moving inwards at the rear of the fuselage.

7 Tailplane design

7.1 Aerofoil selection

The selection of the tailplane aerofoils has been made by considering different characteristics such as the thickness to chord ratio, the drag divergence Mach number M_{DD} and thus the required sweep.

- **Horizontal aerofoil selection**
  According to the literature (6), The t/c ratio of the horizontal tailplane aerofoil should have a 10% lower t/c ratio than the t/c ratio of the wing to delay compressibility effects. Moreover, the horizontal tailplane is subjected to less downwash with the T-tail configuration, therefore is more effective and can be smaller. Using Korn's relation as seen in section 5.4, the M_{DD} and the required sweep of aerofoils can be found.

  As a matter of fact, a symmetrical **NACA0009** aerofoil with a t/c ratio of 9% is selected for its good performance according to literature (6) and to ensure a higher M_{DD} than for the wing.

- **Vertical aerofoil selection**
  The fact that T-tails are typically heavier than conventional tails, as well as issues with weight balance and stability found in later sections, it was decided to choose a vertical tail aerofoil with a high thickness to chord ratio to reduce the empennage's weight. The main downsides of such an aerofoil are the increase in sweep required due to the lower M_{DD} and the increase in wetted area due to a thicker aerofoil. This however also leads to an increase in the horizontal tail lever arm which was a limiting constraint in later sections.

  Therefore, a symmetrical NACA 66(215)-016 aerofoil with a t/c ratio of 16% is selected. As it provides a good compromise between sweep and weight.

  The following table summarises the aerofoils characteristics:

Tail	Aerofoil	t/c (%)	M_{DD}	Required sweep (°)
Vertical	NACA66(215)-016	16%	0.674	39.3
Horizontal	NACA0009	9 %	0.744	19.5

Table 7-1 Tailplane aerofoil selection

7.2 Tailplane placement and sizing

Since stability aspects and stabiliser sizing are closely related, the final design of the tailplane is obtained by multiple iteration between the placement of the tailplane, the placement of the wings, weight and balance aspects and stability considerations.

The relative location of the horizontal tail to the wing is decisive to avoid stall issues and the following graphic is used to visualize feasible locations for the horizontal tail (6):

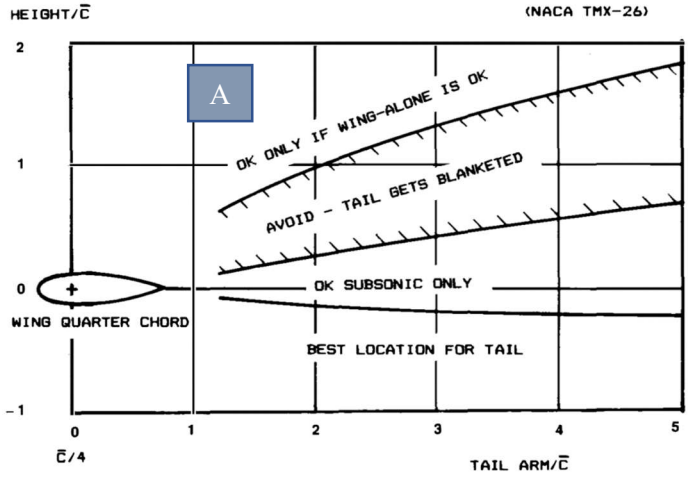

Figure 7-1 Acceptable positioning of the empennage

Since the empennage configuration is a T-tail, the placement must be in the upper zone (zone A). In this zone, one must assure that the wing is able to avoid pitch up without the tail.

- **First estimation of the tailplane sizing and placement**

Now that the tailplane aerofoils have been selected, a first estimation for the stabilisers sizing and placement was obtained by considering the tail volume coefficients (6), thus allowing to calculate the area of the vertical and horizontal tailplanes:
(6)

$$C_V = \frac{S_V.l_V}{S_w.b} \tag{9.1}$$

$$C_H = \frac{S_H.l_H}{S_w.C_{mac}} \tag{9.2}$$

Since the empennage configuration is a T-tail, volume coefficients can be reduced by 5%.Therefore $\boldsymbol{C_v = 0.0855}$ **&** $\boldsymbol{C_H = 0.9}$

As an initial estimation before the final placement of the wings, the horizontal lever arm l_H and the vertical lever arm l_V were assumed to be 50% and 45% of the fuselage length according to literature (6). These approximations also gave initial estimates for the placement of the horizontal tailplane with regards to a $\frac{Height}{mac}$ and a $\frac{tail\ arm}{mac}$ according to figure 9.1. Consequently, a first estimation of the stabilisers reference areas can be calculated using (9.1) and (9.2) $\boldsymbol{S_V = 20.35\ m^2}$ **&** $\boldsymbol{S_H = 24.97\ m^2}$

- **Tailplane sizing and positioning post-wing placement**

These values were used for the initial placement of the wing which allowed for the actual tail arms to be calculated. Due to issues with weight, the placement of the wing for stability was further back than expected. This resulted in significantly smaller lever arms and therefore larger areas and weight than expected. It was therefore decided to place a lower limit on the x location of the vertical tailplane aerodynamic centre. This prevents both the vertical and horizontal tailplane arm (as the vertical tail must support the horizontal tail) from becoming too small therefore stopping the area from becoming unreasonably large.

Fixing the location of the vertical tail aerodynamic centre means that a movement of the wings aft, results in a larger area which causes an increase in span. This methodology resulted in the height of the vertical tailplane and therefore the placement of the horizontal stabilizer with a $\frac{Heigh}{mac}$ = 2.27 and a $\frac{tail\ arm}{mac}$ = 3.45. This is above the region of the wing wake during stall therefore is a possible placement due to the wing's favourable pitch up tendencies as previously discussed.

The vertical placement however is notably much higher than required due fixing the horizontal tail's aerodynamic centre. The total height amounts to 9.8 m which is still close to similar regional aircraft such as the Embraer 170 and can therefore meet hangar requirements (15). Moreover, this is considered as a necessary compromise in order to not have an excessively large tailplane.

- **Vertical and horizontal tailplane ratios**

These placement requirements then defined the aspect ratio of the vertical tailplane to be 0.93, this low aspect ratio allows to reduce the weight impact of the horizontal tail on top of the vertical tail. The taper ratio of the vertical tail was selected at 0.8 which is on the higher end of the typical range in literature (6), as it allows for a more aft placement of the horizontal tail, therefore increasing its moment arm.

An aspect ratio of 4.5 was chosen for the horizontal tailplane which is on the high side, again to allow for a further aft placement. The taper ratio of the horizontal tail plane was fixed to 0.5 to have a fair trade off between aerodynamic efficiency and low weight.

After the final placement of the wing for stability and aerodynamic reasons, the areas of the empennage are: $\boldsymbol{S_V = 30.92\ m^2}$ **&** $\boldsymbol{S_H = 28.63\ m^2}$

The tailplane placement and sizing are summarised in the following table:

Tail	**Aspect ratio**	**Taper ratio**	**Area (m^2)**	**Lever arm** (m)
Vertical	0.93	0.8	$30.92\,m^2$	8.68
Horizontal	4.5	0.5	$28.63\,m^2$	12.78

Table 7-2 Tailplane placement and sizing

8 Fuselage Design

8.1 Cabin and Cargo sizing

To determine the cross section of our aircraft, it was necessary to determine the maximum height and the maximum width of the section. For the width, typical values depending on the number of seats from (16) were used. Different widths obtained: $Wi_{aisle} = 381mm$, $Wall\ thickness = 70mm$ and $Wi_{seat-wal} = 50mm$. To get the width of the seats abreast historical data were used from (3) and we got $Wi_{Two\ Seats} = 1016mm$. It is important to note that all the values concerning the seats were taken considering that they were economic seats. So $\boldsymbol{Wi_{max} = 2653\ mm}$. For the maximum height, information given in the videos recorded were used. Different heights were obtained: $H_{cabin} = 1930mm$, $H_{Cargo} = 1000mm$ and $H_{floor} = 162mm$. So $\boldsymbol{H_{max} = 3232mm}$.

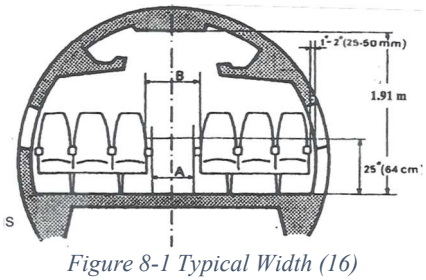

Figure 8-1 Typical Width (16)

To make sure that everything fits into the fuselage, the diameter has been considered equal to the longest dimension. So $\boldsymbol{D_f = 3232mm.}$

Because our aircraft aims to realize only regional transport with not many passengers, the cargo is stored in bulk with no need of Unit Load Devices.

Overhead storages were added to allow each passenger to travel with a baggage in cabin. Dimensions of overhead storage were determined using what the airlines allow as carry-on baggage on average.Finally, the appendix A shows what looks like the cross section.

It is remarkable to see that all the values for the widths have increased. Indeed, they have adapted to a larger diameter imposed by the height.

8.2 Emergency exits and Utilities

The number and type of emergency exits are regulated by FAR25.807. They depend on the number of passengers in our aircraft. Because the plane being designed carries 90 passengers, three emergency exits must be implanted on each side of the plane.

	Type	Min width	Min Height	Max radius	Max Step Height (Inside)	Max Step Height (outside)	
1 Type 1	Floor Level	24	48	8	/	/	inch
1 Type 3	Above wing	20	36	7	20	27	inch
1 Type 4	Above wing	19	26	6.3	29	36	inch

Table 8-1 Emergency Exits

The Type 1 emergency exit was confused with the door through which passengers enter. The minimum width required for this emergency exit is the width required for a crew cabin station. For the other two emergency exits over the wings, additional space was required between the rows of seats to let passengers out in case of emergency. The minimum width for each emergency exit has been added in front of each row of seats facing an emergency exit.

To respect the density of one lavatory for 50 passengers, two lavatories were added in the plane. One at the beginning of the passenger cabin and the other at the end. On average, a lavatory requires a surface of $1m^2$. (2)

To accommodate all 90 passengers, the seats were arranged in 23 rows of four seats each. The rows are composed of 2 seats abreast on each side of the central aisle. This distribution requires two cross aisles, one at the beginning of the cabin and one at the end. (2)

Since the plane is supposed to be a short flight, the volume allocated per passenger in the galleys is $1ft^3$. This corresponds to about 2.5 m^3 for all passengers.

All these needs have had an impact on the global organization of the passenger cabin and in particular the length of this cabin.

8.3 Seating Layout and Length

Considering all the previous elements, the organization of the passenger cabin has been decided.

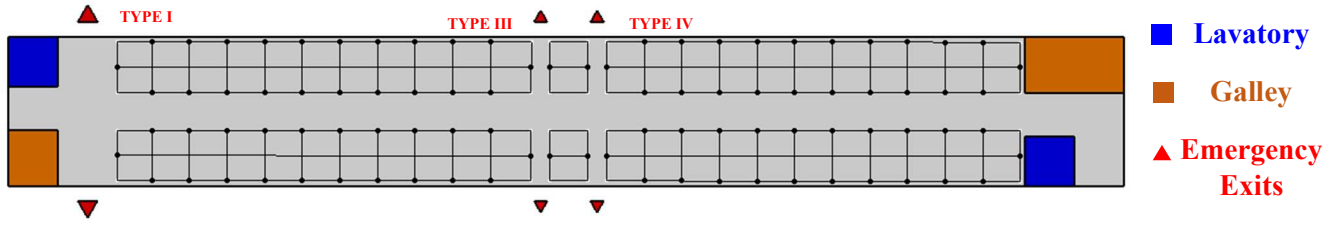

Figure 8-2 Seating Layout

The total length of the passenger's cabin can be therefore calculated.

$$L_{cabin} = 23 * L_{Seat\ pitch} + 2 * L_{lavatory} + 2 * L_{cross\ aisle} + Wi_{Type\ III} + Wi_{Type\ IV} \qquad (10.1)$$

With: $L_{seat\ pitch} = 762mm$, $L_{lavatory} = 1000mm$, $L_{cross\ aisle} = 1000mm$

So $\boldsymbol{L_{cabin} = 22517mm}$.

An empirical law was also used to verify the length found. This law relates the seat pitch multiplied by the number of seats divided by the number of seats side by side to the length of the cabin. This empirical law can be found in appendix B.

A length of 22860mm was obtained, which represents a deviation of 1.5% from the value found. Thus, the value found is consistent.

8.4 After Body sizing

The afterbody has been designed to minimize the drag it causes. By following the graph below, an approximate length of the tail is obtained.

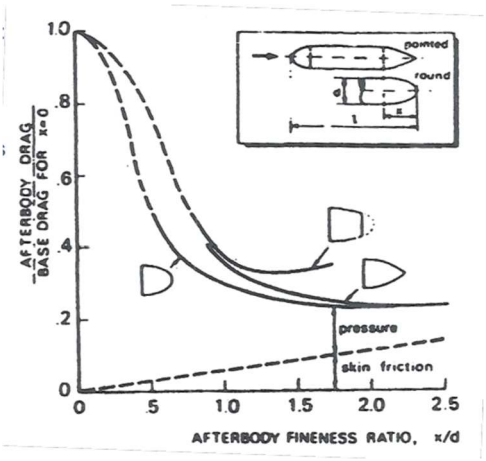

Figure 8-3 Empirical Law to determine the fitness ratio of the afterbody (16)

To obtain the least drag possible, the fitness ratio should be chosen between 1.5 and 2. 2 was chosen even if it increases the skin friction a bit because you need an afterbody big enough to support the tail. Knowing the diameter, it is possible to obtain the length of the tail. So, $\boldsymbol{L_{After\ Body} = 6463mm}$. This also reduces the sweep of the afterbody which is better to minimise the drag. So $\boldsymbol{\theta_{sweep} = 21°}$. In addition, a good way to optimise space is to fit part of the passenger cabin into the afterbody.

Knowing all the above, here is a representation of the tail.

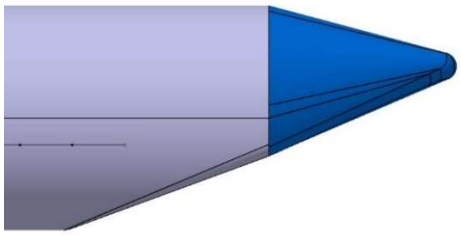

Figure 8-4 Illustration of the After Body

8.5 Nose and Cockpit sizing

Ensuring that Mdd is equal to the maximum Mach during cruise, provides the length of the nose.

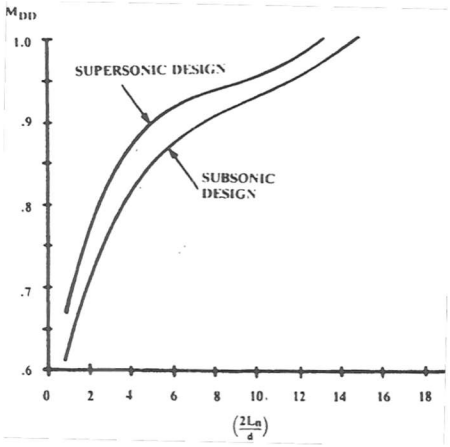

Figure 8-5 Relation between Mdd and nose fitness ratio

Indeed, for an Mdd of 0.72 we obtain a fitness ration for the nose of 1.05. The length of the nose can therefore be obtained. $\boldsymbol{L_{nose} = 3393mm.}$

To design the rest of the nose, it is necessary to have that the cockpit fits well in the nose and that the pilots can see enough around them. Several angles need to be respected:

- the angle of vision downwards in front: 20° (6)
- angle of vision downwards on the sides: 35° (6)
- angle of vision in the horizontal plane: 125° (2)

For the pilots to fit into the seat, certain distances must be respected:

- Total width between the two pilot seats: 1880mm (2)
- Height of a pilot seated + height of a seat: 1317mm (2)
- Depth of a cockpit: 1111mm (2)

A simplified geometry of the cockpit could look like this:

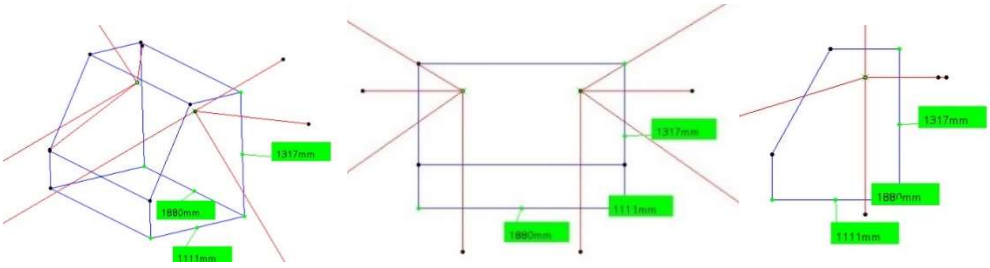

Figure 8-6 Iso, Front and Side view of a simplified geometry of the cockpit

The red lines highlight the angles to be respected. The blue lines highlight the distances to be respected.

Finally, a rough idea of what the nose looks like could be made.

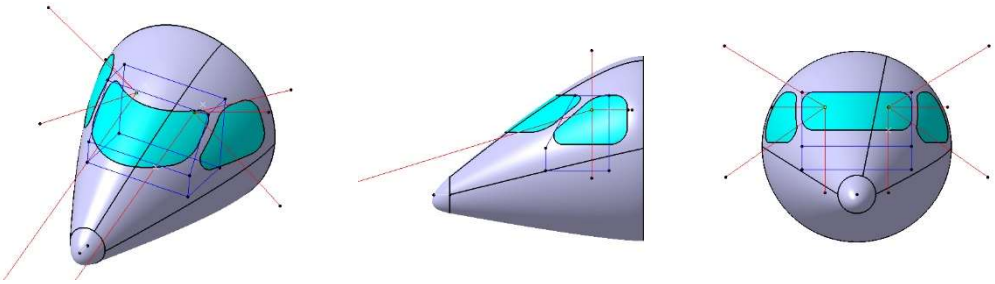

Figure 8-7 Iso, front and side view of the nose

8.6 Summary of data

Data	Value	Unity
D_f	3.2	m
$Wall\ thickness$	0.07	m
L_{nose}	3.4	m
L_{cabin}	22.5	m
$L_{afterbody}$	4.8	m

Table 8-2 Table summarizing fuselage data

9 Aircraft Systems Design

9.1 Fuel System

The fuel chosen is Jet A-1 because it is the most common fuel for transport aircraft. According to ASTM D1655, the density of Jet A-1 varies between 775.0 and 840.0 kg/m^3. From the maximum density and the fuel weight W_f, the required volume for the tanks is $\boldsymbol{V_{fuel} = 19.81\ m^3}$ (added 2% to make sure the open ventilation is working, see below).

The main tanks in a transport aircraft are in the wings. The volume available in the wings is dependant of the placement of the spars in it. In the case of this aircraft, the front and rear spars are placed respectively at 12% and 67% of the wing chord. The wing tanks are then designed to suit the wing aerofoil (see figure below).

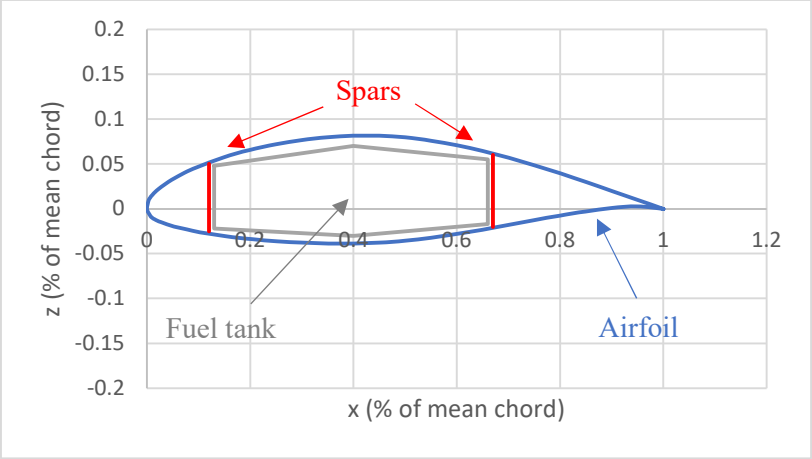

Figure 9-1 Fuel tank form in the wings

The volume available in the wings is then:

$$V_{wings} = 2 * Area_{mean} * L_{wing,available} \qquad (11.1)$$

Where $L_{wing,available}$ is the length of the wing minus the space needed by the undercarriage (2.2m se paragraph 12.1) and minus 0.5m at the wing tip to put a surge tank. The calculated volume available in the wings is $V_{wings} = 13.17\ m^3$.

Since the aircraft have rear fuselage mounted engines, a feeder tank next to the engines is required. The feeder tank has been designed to be able to provide fuel to the engines for 5 minutes at maximum thrust: $V_{feeder\ tank} = 0.79\ m^3$.

The rest of the fuel is stored in the centre tank which is a tank in the fuselage under the floor and in the continuity of the wing. The volume of this tank has been designed by geometry to allow the undercarriage to retract itself in the fuselage.

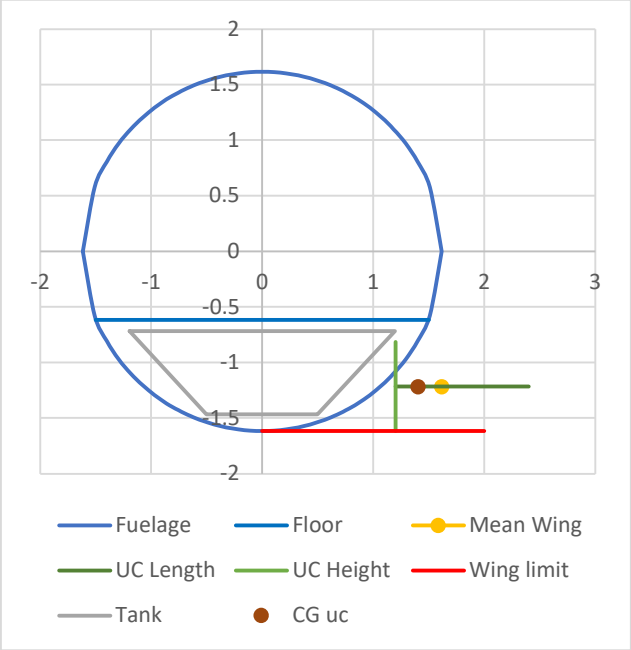

Figure 9-2

The width of the centre tank is 4.60m and was determined to meet the volume of fuel required, therefore $V_{centre\ tank} = 5.85\ m^3$. The volume available for the fuel is then:

$$\boldsymbol{V_{available}} = V_{wings} + V_{feeder\ tank} + V_{centre\ tank} = \mathbf{19.81\ m^3}$$

All the tanks have an open vent system which connect the ullage in each tank to the outside air. The ventilation system is important because it prevents the fuel from evaporating. The reduction in pressure due to the increase in altitude leads to a decrease in the boiling point of the fuel which can then evaporate.

To transfer the fuel from tank to tank 2 transfer pumps are used for each tank (1 is for redundancy) and especially to transfer the fuel from the wing tanks and the centre tank to the tank next to the engines. While 2 booster pumps are used to send the fuel from the tank next to the engines to the engines. As the aircraft's 2 engines are located at the back and not near the wings, a weight penalty is included in the total weight of the fuel system.

With the aim of improving safety on board the aircraft, it contains a fuel Jettison system to drop fuel to reduce the weight of the aircraft in the event of a take-off incident in order to be able to land quickly.

These tanks will provide fuel to both engines and the APU. A diagram of the fuel tank and system layout can be found in the Appendix D.

9.2 Flight Control System

(17) The fly-by-wire system with an electronic interface of an airplane replaces the old human-controlled system with mechanical links. Main advantages of the fly-by-wire system are: reduce aircraft weight, improve reliability and more effective control. As the use of this system is becoming increasingly reliable and sought after, the aircraft will be equipped with it. On top of that, the fly by wire system allows for the use of spoilers, which provides greater roll control.

Due to the T-Tail the stall is abrupt, so the pilot and co-pilot need to be extremely aware when the aircraft is close to stall. That is why the aircraft is equipped with a stick shaker to warn them. Each stick is composed of an electric motor

of 0.3A and 12V. The whole unit will not exceed 0.02 m^3 and a weight of 2kg (18). Since these values are minimal compared to the overall electrical system, no weight penalty was considered.

9.3 Electrical System

The electrical system of the aircraft is expected to require 75 kW during cruise. This value was determined by comparing different aircraft, including the CRJ900. This aircraft is also equipped with a fly-by-wire system and is powered by 2 generators of 40 kVA each (19). As the CRJ900 was manufactured in 1999, the electrical components have become more efficient but more energy intensive. Therefore, assuming a power factor of 0.75, the power required by the aircraft has been estimated at 100 kVA (an increase of 25% which also takes into consideration that the number of electronic systems replacing the previous hydraulic systems will be more numerous).

To reach the power requirement, each engine has a 50 kVA Integrated Drive Generator (IDG) and two generators are attached to the APU providing a total power of 60 kVA (20). In the case of an emergency, a Ram Air Turbine (RAT) generates 5 kVA (like the A220 because of the sizing resemblance (21)) to assure back-up power generation and a battery capable of maintaining the electrical system working for 30 minutes is installed.

During the cruise the engine generators are sufficient to provide the necessary power for the electrical system. In the event of an engine failure, one engine generator and the APU can together support the required power.

While the aircraft is on the ground, a ground power unit (GPU) is made available to it at the front, supplying it with 90 kVA 115V 400Hz.

To be able to supply all systems and sub-systems with the correct voltage, the electrical system must be able to provide 115V 400 Hz AC and 28V DC. A table to resume all systems and voltage requirements is presented below:

Voltage	System
115 VAC 400 Hz	Power generation: IDG, APU & RAT
115 VAC	Landing gear, Cabin pressurization, Pneumatics
28 VDC	Avionics, Anti-icing, Lightning, APU start

Table 9-1 Summary of systems and voltage requirements

To be able to supply 28 VDC, the aircraft is equipped with 2 (for redundancy) Transformer Rectifier Units (TRU) as well as state converters (VSCF systems) to maintain a constant frequency of 400 Hz for the AC power generation.

Standby Flight Instruments and Aircraft Emergency Floor Path Illumination have their own backup power supplies in compliance with EU-OPS 1.652.

9.4 Pneumatic System

Pneumatics use bleed air from the engines and the APU. This is used for the environmental control system, the anti-icing system and the thrust reversers.

9.4.1 Environmental Control System

Pressurized cabins and compartments to be occupied must be equipped to provide a cabin pressure altitude of not more than 8,000 feet at the maximum operating altitude of the airplane under normal operating conditions. [FAR 25.841] This is made possible by an Environmental Control Unit (ECU) that can also regulate the temperature and humidity of the cabin by means of sensors. (22)

9.4.2 Anti-icing System

Ice on the leading edges of the aircraft (wings, nacelle, empennage) can have disastrous effects on the aircraft. In accordance with FAR25.1419, the aircraft is equipped with an anti-icing system. It uses the hot air coming out of the

engines and the APU (pressure of 20 to 25 PSI) (2) to heat the leading edges of the aircraft. Sensors are present to prevent overheating.

9.4.3 Thrust reverser

Brakes represent a significant cost in the maintenance of an aircraft. Any system that preserves them is appreciated. Especially as aircraft tend to become more aerodynamic and therefore have more and more difficulty slowing down on landing. Therefore, the aircraft is equipped with thrust reversers producing a drag of almost 40% of the thrust of our engines during landing roll. (2) The launch of the thrust reversers is achieved through the bleed system, making our bleed system more complex (a weight penalty has been applied).

10 Structural Layout

10.1 Fuselage

For this part, frames and spars must be provided to maintain the cylindrical shape of the fuselage and allow the forces to be distributed throughout the structure of the aircraft. In addition, a floor had to be attached to the fuselage to support the weight of the passengers and equipment. For this floor, two very solid spars cross the plane in all its length, and they come to be attached on the frames with smaller beams. A skin is placed on top of these structural elements. It allows to resist to pressure, bending, shear and torsion loads. Some parts of the fuselage had to be reinforced more than others because they were subjected to more important loads. It was the case for the frames which supported the wings as well as the frames which supported the two engines at the back of the plane. For these parts heavy frames have been provided to be more resistant.

By looking at historical data, the dimensions of the structure could be determined.

- Density of frames: About one every 50 cm. (23)
- Frames thickness: 1.2mm
- Density of stringers: Around one every 25°.
- Stringer's thickness: 1mm

Stringers and frames all have C shapes. Indeed, this shape allows to keep the mechanical properties but makes the structuring elements lighter. For stringers, this C-shape allows the connection between the outer skin and the inner skin. For the frames, this C shape, allows the passage of the stringers and the link of the floor to the frames.

A simplified version of the structure can be seen in appendix C.

10.2 Wing

The wings require several ribs to maintain the aerodynamic shape and provide access to attachment points for various elements on the wings. On top of these ribs, a skin is grafted to resist the efforts of torsion, bending and pressure. Finally, spars are needed to bind all the ribs together and transfer the forces undergone by the wing to the fuselage.

One of the main dimensioning elements for the wings is the fact that the main landing gear are supposed to fit in the wings. It is also important to leave room for the fuel tank. Two spars are thus necessary in the wings to leave enough space. In the case of several spars in one wing, the first one should be between 12 and 18% of the average chord and the last one should be between 55 and 70% (2). Because high lift devices requirement 10% of the beginning of the wing and 25% at the end of the wing, the first spar was placed at 12% and the last one at 67%.

To create a good path of the constraints and to avoid that all the efforts are concentrated in places too small, a bending beam was added inside the fuselage to connect the two wings in the continuity of the spars. This will allow to minimize the mass of the load path while improving the resistance to the efforts of the structure.

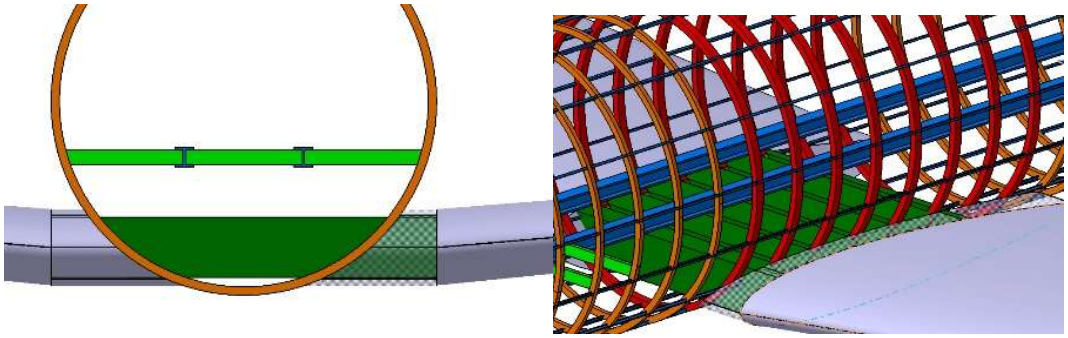

Figure 10-1 Spar and Bending beams for the wings

In addition, due to the presence of winglets on the wings, the spars will continue in the wings to ensure a good mechanical hold.

10.3 Tail

The wings are smaller for this part, but the structures are the same. Ribs ensure the good aerodynamic shape; a skin comes to cover these ribs to ensure a good distribution of the undergone efforts. It was conceivable to think that the number of spars would change. Indeed, there was no need to leave room for landing gear or fuel tanks. However, the aerodynamic forces on the wings of the tail are more important because they are in the turbulent flow of the aircraft. In addition, the vertical T tail must support both horizontal control surfaces. It is therefore necessary that it is solid. Thus, two spars were put in the two horizontal wings and in the vertical stabilizer.

The starting points of the vertical tail spars have been set at 15% and 60% of the root cord to leave enough room for the control surfaces. The end points of the spars are placed so that they intersect the horizontal tails to connect their spars to the vertical tail spars. For the spars of the horizontal tails, their starting point is the intersection of the horizontal tails with the vertical and their end points are placed respectively at 15 and 60% of the tip cord.

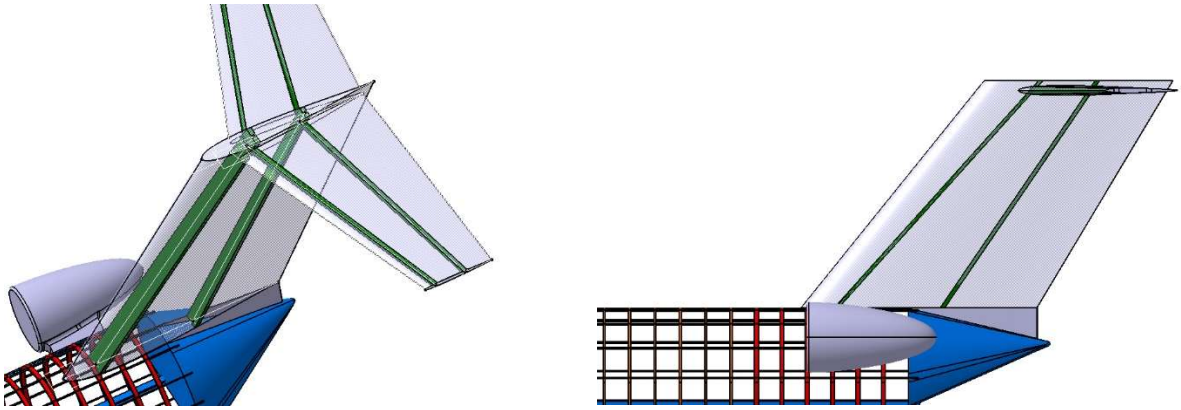

Figure 10-2 Spar of the Tail

10.4 Materials

When choosing materials, two parameters must be considered: mass and resistance to stress. Nowadays, the most common material is aluminium structural elements and composite skins. The use of composites allows to save mass. In addition, composites have better mechanical properties than aluminium. One of the most common composites is carbon fibre. Even though carbon fibre is more expensive than aluminium, the mass gain it provides allows for fuel savings and thus offsets its own cost. Finally, titanium was chosen for the undercarriage because these systems need to be extremely shocked resistant.

Component	Materials
Fuselage	Al-7050 (24)

Skin	Carbon fibre
Undercarriage	Ti-6Al-4V (25)

Table 10-1 Materials of different components

To represent the impact of the choice of materials, penalties have been applied or not in the Weight and Balance section.

11 Undercarriage Design

The placement and sizing of the undercarriages was done iteratively in parallel with the placement of the centre of gravity and the placement of the wings. The values presented in this section reflect the last iteration of this process.

11.1 Requirements and position

To design undercarriages, one of the main things is to know what is acceptable for the airports where the aircraft will land. As shown in figure 12.1, most airports impose a tyre pressure limit of 254 psi. Indeed, the X in the PCN of each airport stands for 254 psi limit pressure.

	Runway	TODA (m)	LDA (m)	PCN
Wellington (NZWN)	16/34	2,300	1,815	64 F/B/X/T
Christchurch (NZCH)	02/20	3,288	3,288	60 F/B/X/U
Hamilton (NZHN)	18L/36R	2,119	2,059	45 F/C/X/T

Figure 11-1 Airport description

In addition, the number of wheels per strut depends on the MTOW. Thus, an MTOW of about 107000lbs imposes two wheels per strut for a tricycle configuration. Finally, as a tricycle configuration has been chosen three struts will be present on the aircraft.

To position the main undercarriage, three angles needed to be satisfied: Overturn Angle, Tip Back Angle and Vertical CG Angle. To get a good overturn angle a rear tilt of 10° has been added to the fuselage to move forward the point of contact. To clarify the table 12.1, the x's originate from the nose of the aircraft and are percentage of the fuselage length while the y's and z's originate from the centre of the fuselage and are percentage of the radius of the fuselage. The y position has also been designed to allow the undercarriage to retract into the fuselage.

	Nose	**Main**
X (%L)	10	62.51
Y (%R)	0	1.49
Z (%R)	-1.74	-1.74

Table 11-1 Position of the Undercarriages

Thanks to the previous positions and the dimensions of the aircraft it is possible to obtain the dimensional angles and to verify the veracity of the undercarriage placements.

	Value	**Constraint**
Tipback angle [°]	10.02	10 – 15 °
Vertical CG angle [°]	10.29	> Tipback Angle
Overturn angle [°]	44.08	< 63 °

Table 11-2 Dimensional Undercarriage angles

11.2 Loads

Two types of loads must be calculated to take everything into account: static load and dynamic load. However, it is important to note that the dynamic load only applies to the nose undercarriage.

Furthermore, by looking at the values of other similar aircraft, the weight distribution between the main undercarriage and the nose undercarriage could be determined. Thus, 8% of the MTOW rests on the nose undercarriage while the rest

rests on the main undercarriage (2). The nose undercarriage supports 3900kg and the two hand undercarriages support 44887 kg.

$$W_{static} = \frac{Static\ Load\ On\ Strut * 1.07}{Number\ of\ Wheels\ per\ Struts} \quad (13.1)$$

$$W_{dynamic} = \frac{Deceleration * H * W_0}{g * B} \quad (13.2)$$

With a deceleration of $10ft/s^2$, B the distance between the nose undercarriage and the main undercarriage along the fuselage and H the height of the CG from the ground line.

Landing Gear	Static Load [lb]	Dynamic Load [lb]	Maximum Load [lb]
Nose	4549	6106	10700
Main	26416	N/A	26416

Table 11-3 Landing gear Loads

11.3 Selection of tires

Now that the loads on the undercarriage are determined, it is possible to choose the right tyres. To do this, both the maximum permissible pressure and the maximum load must be respected to find a suitable tyre. It has always been necessary to take the smallest possible tyre for a given value set to minimise the weight of the tyre. In addition, the type of tyre is important. There are indeed several types of undercarriages possible, three-part, type I, type II, type III, type VII, metric and radial.

The three parts were chosen because they are relatively small and very efficient and are used by other jet transport aircraft similar to our aircraft. (26)

The table 12.4 summarize the parameters of the chosen tires.

Landing gear	Model	Ref	Rated Loads (lbs)	Inflated Diameter (in)	Inflated Width (in)	Rated Inflation (psi)	Rolling radius (in)
Nose	Three Part	249K83-3	12200	24	9.5	160	9.85
Main	Three Part	61B-3912-TL	28300	35	11.5	255	14.8

Table 11-4 Tire description

The maximum pressure allowed is 255psi which is higher than the limit set by the airport but the rated load we get is higher than what we need. The main gear tyres will therefore not be inflated to the maximum pressure but a little lower to respect the airport rules. This will reduce the acceptable rated load a little but will still be sufficient to support the previous one.

11.4 Shock Absorber Sizing

Now that the tyre dimensions are found, and the loads are known it is possible to size the shock absorbers for the undercarriage. Shock absorbers are necessary because a simple strut couldn't handle the load of a landing and would break. Therefore, adding shock absorber on each landing gear is mandatory. Having an efficiency of about 80% (2) and being used in most jet transport aircraft, oleo-pneumatic shock absorbers have been chosen. The first thing to determine to start sizing the shock absorbers is to calculate their stroke.

$$S = \frac{{V_v}^2}{2g\eta N_g} - \frac{\eta_T}{\eta} S_T + 1Inch \quad (13.3)$$

Where $\eta = 0.8$, $\eta_T = 0.47$, $V_v = 10\ ft/s$ and $N_g = 2.7$ are constant value. So, the only value which still need to be determined is S_T. To do so, the diameter of the tire and the rolling radius must be used. Indeed $S_T = \frac{D}{2} - R_r$.

Once the stroke is obtained, the oleo needs to be sized. The stroke is used to determine both the length of the oleo and the outside diameter.

$$L_{min-oleo} = 2.5S \qquad (13.4)$$

$$D_{oleo} = 0.04\sqrt{L_{oleo}} \qquad (13.5)$$

In addition to the length given by (10.4), an extra 15% must be added to the length (2) to allow for the compressed gas chamber. The next table summarize the value found.

	S (m)	D_{oleo} (m)	L_{oleo} (m)	Overall Length (m)
Main	0.230	0.105	0.661	1.2
Nose	0.230	0.165	0.661	1.13

Table 11-5 Dimensions of the shock absorbers and struts

11.5 Undercarriage Design

The undercarriage retraction system is designed so that the main undercarriage retracts into a part of the wing and into the fuselage. To realise this system, the space needed for the fuel tank inside the fuselage and the space available in the wings has been considered. Once the main undercarriage is deployed, it remains upright and to help guide the shock absorber an arm links the shock absorber and the wheel axle.

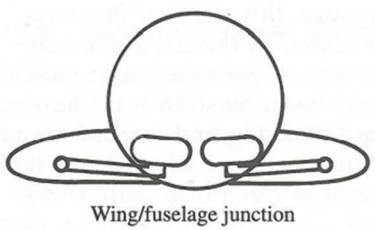

Figure 11-2 Illustration of the retractable main gears

For the nose gear, the system is different. The gear will retract into the nose in the direction of the aircraft's movement. In order to avoid the landing gear having difficulty extending in strong winds, it is necessary to open the landing gear in such a way that the door is assisted in opening. (2)

11.6 Runway Suitability

Now that all the undercarriage parameters are known, it is necessary to verify that the aircraft can operate on its mission profile airfields. To do this, the ACN of the aircraft must be obtained and compare it to the most constraining PCN.

As shown in Figure 10.1 the most constrained airport is Hamilton. Indeed, the ACN found must be smaller than the airport's PCN and Hamilton has the smallest PCN.

To find the ACN, COMFAA was used. The software can give the ACN of the aircraft for different hardness of airfield.

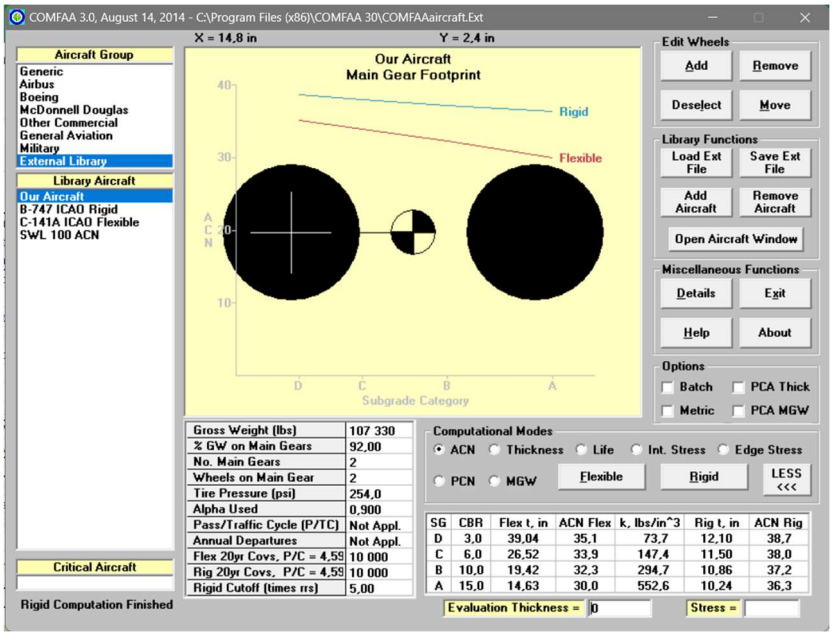

Figure 11-3 COMFAA settings

Figure 12.3 shows that the ACN of the aircraft is 33.4 for a hardness of C which is inferior of the PCN of Hamilton airport, so the aircraft can operate on all runways without being damaged.

11.7 Iteration

All the values presented in this section were obtained through an iterative process. The undercarriages are related to the position of the wings and their placement depends on the position of the global centre of gravity of the aircraft. To find the right position of the undercarriage, the position of the wings, the position of the centre of gravity, the stability, the dimensional angles etc. had to be taken into account. The process was long, and some compromises had to be made to try to satisfy all these requirements as best as possible. For example, the x-position of the main undercarriage is a bit too close and complicate the realisation of the retraction system, but this allowed to converge towards a coherent whole.

12 Weight and Balance

To determine the centre of gravity for the aircraft, a weight estimation for all sub-systems is presented below.

12.1 Weights Estimation

The methods used are a combination of those provided by Raymer (6) and Torenbeek (16). Since the methods are made for a fully conventional aircraft, it is important to precise a couple of assumptions:

- The aircraft has winglets on its wings, a weight estimation has been done separately.
- The nacelle must be sized to allow the use of thrust reversers. According to (27) (27) 30% of the weight nacelle is allocated to this. A weight penalty of $\frac{1}{1-30\%} = 1.43$ has been therefore applied.
- The aircraft engines are placed at the back of the fuselage so all the fuel system will be larger to transport the fuel from the wing tanks and from the centre tank to the feeder tank. Adding to that the use of a fuel jettison system, a weight penalty of 1.25 have been applied as well as a shift backward for the fuel system centre of gravity.
- The fudge factors linked to the materials used were taken very conservatively, including a fudge factor of 1.67 for the undercarriage since the latter is made of titanium which is 67% heavier than the aluminium (see paragraph 12.4). (28)

12.2 Balance analysis

A summary of all weight and centre of gravity is presented table 14.1. The x axis is along the fuselage length and begins at the nose and the z axis is along the fuselage width, begins at the middle of the fuselage diameter and looks upward. The positions of systems have been estimated with to the location of main components of the according system.

Notice that the fuel system centre of gravity along the x axis is 0.64 while the centre of gravity of the wing and centre tanks alone is 0.59. To better stability results all baggage is placed under the floor, between the nose of the aircraft and the fuel centre tank and should not take more than 5.8 m (allowing a volume of 7.65 m^3 assuming a density of 200 kg/m^3 for the baggage) (2). Therefore, in order to shift the overall centre of gravity forward the electric and air-conditioning systems are placed between the baggage and the centre tank with a volume of 7.12 m^3 available (29).

With the empty weight and the centre of gravity for this configuration determined, the variation of the overall centre of gravity have been calculated considering the adding of payload and fuel. The calculations are summarized in a form of a graph presented below.

System	Mass (kg)	x_{CG} (% of $L_{fuselage}$)	z_{CG} (% of $D_{fuselage}$)
Aircraft Wings	3190	0.61	-0.41
Winglets	175	0.63	0.29
Horizontal Tailplane	533	1.02	2.09
Vertical Tailplane	355	0.97	1.02
Fuselage	5175	0.47	0.00
Main Landing Gear	1671	0.63	-0.38
Nose Landing Gear	303	0.10	-0.37
Nacelle	1268	0.80	0.30
Installed Engines	4029	0.80	0.30
Engine Controls	55	0.06	-0.03
Engine Starters	66	0.80	0.30
Fuel System	303	0.64	-0.64
Flight Controls	741	0.62	-0.03
Installed APU	238	0.90	0.00
Instruments	136	0.06	-0.03
Hydraulic System	118	0.67	0.17
Electrical System	733	0.30	0.00
Avionics	835	0.06	-0.03
Furnishings	1852	0.48	0.00
Air-Conditioning	388	0.30	0.00
Anti-Icing System	98	0.58	0.30
Handling Gear	15	0.13	-0.25

Table 12-1 Summary of all weight and centre of gravity for systems

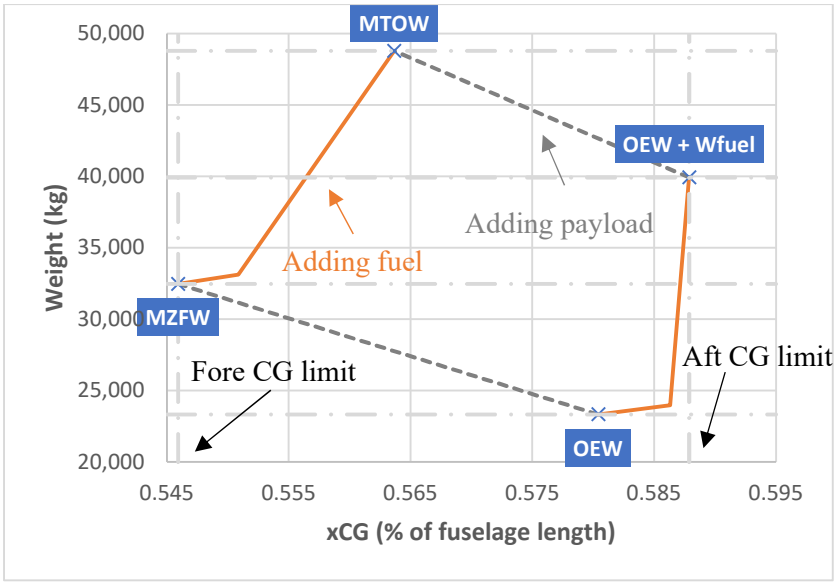

Figure 12-1 Summary of centre of gravity position

13 Aerodynamic Analysis

13.1 Zero Lift Angle of Attack of Wing

The zero lift angle of attack of a wing can be calculated from the aerofoil zero lift angle of attack (-3°) according to the equation (16.1) by considering twist with a correction for Mach number. The 2nd (change in zero lift angle of attack per unit of twist) and 3rd (Mach number correction) terms are taken from figures 16.1 and 16.2 at the closest taper (0.5) and aspect ratio (>6) for the twist correction.

$$\alpha_{0,w,clean} = \alpha_0 + \frac{\Delta\alpha_0}{\varepsilon_t}\varepsilon_t \frac{\alpha_{0,at\ M}}{\alpha_{0,at\ M=0.3}} \tag{16.1}$$

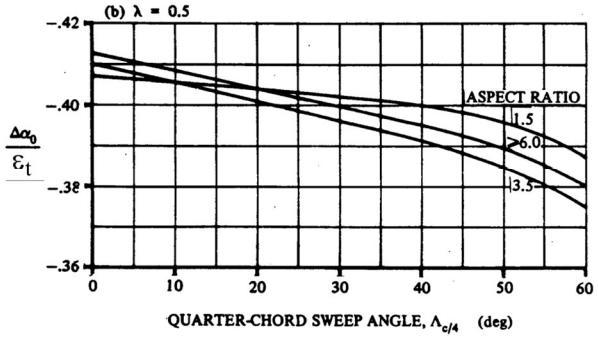

Figure 16-1 Selection of the zero lift angle of attack per unit of twist

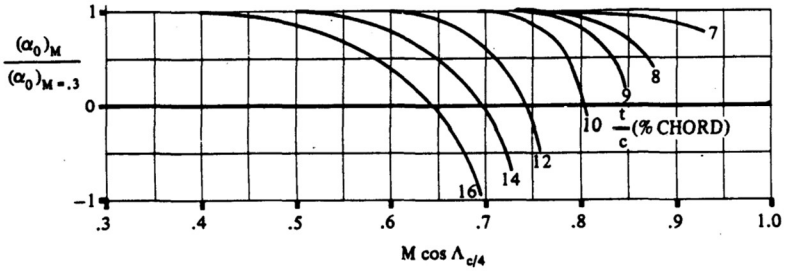

Figure 16-2 Selection of the Mach number correction term

Additionally, during take-off and landing the extension of flaps results in a change of the zero-lift angle of attack according to equation (16.2). $(\Delta\alpha_0)_{airfoil}$ is taken to be -10° for take-off and -15° for landing.

$$(\Delta\alpha_0)_{wing} = (\Delta\alpha_0)_{airfoil}\left(\frac{S_{flapped}}{S_{ref}}\right) \tag{16.2}$$

This gives the following values for zero lift angle of attack during different mission segments.

Take-off	W-C Cruise	C-H Cruise	H-W Cruise	Loiter	Cruise Missed approach	Landing
-8.01	-2.32	-2.35	-2.35	-1.77	-2.44	-11.13

Table 16-1 Zero lift angles of attack for each mission segment

13.2 Lift Curve Slope of Wing

The lift curve slope of the whole wings in a clean configuration is given by equation (16.3) with the aerofoil efficiency factor (η) and fuselage (F) spill over factor given by equations (16.4). If the product of exposed area to reference area, multiplied by the fuselage spill over factor exceeds 1, it is set to 1 instead.

$$(C_{l_\alpha})_{clean} = \frac{2\pi A}{2+\sqrt{4+\frac{A^2\beta^2}{\eta^2}\left(1+\frac{\tan^2\Lambda_{max,t}}{\beta^2}\right)}}\frac{S_{exposed}}{S_{ref}}F \tag{16.3}$$

$$\eta = \frac{\beta C_{l_{\alpha|M}}}{2\pi}, \quad F = 1.07\left(1+\frac{D_f}{b_f}\right)^2 \tag{16.4}$$

During take-off and landing, flaps are deployed which affect the wings lift curve slope as in equation (16.5).

$$(C_{l_\alpha})_{\frac{TO}{l}} = (C_{l_\alpha})_{clean}\left(1+\left(\frac{c'}{c}-1\right)\left(\frac{S_{flapped}}{S_{ref}}\right)\right) \quad (16.5)$$

The final lift curve slopes of the wing can therefore be found at all segments as seen in table 16-2 in (1/rad).

Take-off	W-C Cruise	C-H Cruise	H-W Cruise	Loiter	Cruise Missed approach	Landing
5.86	6.25	6.34	6.37	5.68	6.41	5.88

Table 16-2 Lift curve slopes of the wing for each mission segment

13.3 Maximum Lift Coefficient of Wing

The maximum lift coefficient at cruise corresponds to the maximum lift coefficient of the clean wings as flaps are not deployed. This was calculated in chapter 7.1 using equation 7.2. The maximum lift coefficient at landing, as the most constraining condition is given by the achieved maximum lift coefficient due to high lift devices while the maximum lift coefficient at take off equals 80% of the landing maximum lift coefficient. These values are summarized in table 16-3.

Take-off	Cruise	Landing
2.401	1.509	3.002

Table 16-3 Maximum lift coefficients of the wing

13.4 Aerodynamic Analysis of Tailplane

The aerodynamic properties of the tailplane are calculated using the same methodology as for the wing. As the horizontal tailplane has no twist, and has no flaps, according to equations 16.1 and 16.2 the zero-lift angle of attack is taken to be the aerofoil's zero lift angle of attack. As the aerofoil is symmetric, this gives a value of 0°. The maximum wing lift coefficient is found from equation 7.2_ which accounts for 3D affects and sweep. This is the same for all flight segments as there are no high lift devices. The horizontal tailplane has no high lift devices therefore the maximum lift coefficient is simply that of the clean wing. The lift curve slope is calculated again with equation 16.3. All values are summarized in table 16-4.

α_0	0						
$(C_{l_{max}})_{clean}$	1.111						
	Take-off	W-C Cruise	C-H Cruise	H-W Cruise	Loiter	Cruise Missed approach	Landing
C_{l_α}	3.821	4.570	4.619	4.636	4.245	4.657	3.834

Table 16-4 Aerodynamic properties of the tailplane

14 Drag

14.1 Components of Drag

The total drag of the aircraft is given by the sum of zero lift drag, wave drag, and lift induced drag as summarized in equation (17.1).

$$C_D = C_{D_0} + C_{D,wave} + C_{D_i} \quad (17.1)$$

14.2 Zero Lift Drag

The zero lift drag of an aircraft can be calculated by summing the drag of all major components and other miscellaneous drag terms. This is known as the component build up method as it given by equation (17.2) with all terms explained in table 17-1. A summary of all quantities for all mission segments is given in appendix.

$$C_{D0} = \sum C_{f,c} * FF_c * Q_c * \frac{S_{wet,c}}{S_{ref}} + C_{D,misc} + C_{D,L+P} \quad (17.2)$$

$C_{f,c}$	Skin friction coefficient	FF_c	Form factor	Q_c	Interference factor
$\frac{S_{wet,c}}{S_{ref}}$	Wetted area ratio	$C_{D,misc}$	Miscellaneous drag coefficient	$C_{D,L+P}$	Leakages and protuberances drag coefficient

Table 17-1 explanation of notations

14.3 Wetted Area Ratio

As the reference wing area has long been fixed, the determination of the area ratio is dependent on the wetted area of each component. The wetted area of the wing and tail surfaces is given by equation (17.3) for a constant thickness to chord ratio wing. An expression for fuselage wetted area is given by equation (17.4) with a fuselage fineness ratio (λ_F- length of fuselage divided by its diameter) of greater than 4.5. equations for the wetted area of the nacelles is given in appendix J. the dimensions of which were based on the geometry of a similar engine (PW1100) of the same family, scaled to the correct dimensions.

$$S_{wet,F} = 2S_{exp}\left(1 + 0.25\left(\frac{t}{c}\right)\right) \tag{17.3}$$

$$S_{wet,F} = \pi d_F l_F \left(1 - \frac{2}{\lambda_F}\right)^{\frac{2}{3}} \left(1 + \frac{1}{\lambda^2{}_F}\right) \tag{17.4}$$

The exposed area is the area of the wing not covered by the fuselage. Therefore, knowing the dimensions of the fuselage as well as other quantities such as taper ratio, S_{exp} could be calculated. The wetted area of the pylons used to hold the engines is calculated as 20% of the nacelles area and added to the total nacelles S_{wet}. Due to its complex and rough sizing, the wetted area of the winglets was found using a CAD software of an appropriate winglet scaled to appropriate dimensions.

14.4 Skin Friction Coefficient

The skin friction coefficient of each component is given by equation (17.5) for laminar flow and by equation (17.6) for turbulent flow. The Reynolds number for each component at each Mach number was calculated with the characteristic length of the wing and tail surfaces being the mean aerodynamic chord while, and the length of the fuselage and engine nacelles. An addition cut-off Reynolds number was calculated given by equation (17.7) to account for skin roughness. A value for k of $0.634*10^{-5}$m was assumed as the commercial design specification makes smooth paint the most appropriate choice. If the cut-off Reynolds number was lower than the actual Reynolds number, the cut-off Reynolds number was taken for the turbulent equation. This however wasn't the case for any of this design's calculations.

$$C_f = \frac{1.328}{\sqrt{Re}} \tag{17.5}$$

$$C_f = \frac{0.455}{(Log_{10}Re)^{2.58}(1 + 0.144 * M^2)^{0.65}} \tag{17.6}$$

$$Re_{cutoff} = 38.21 * \left(\frac{l}{k}\right)^{1.053} \tag{17.7}$$

Equation 17.6 and 17.7 were weighted in order to consider the proportion along each component for which flow is turbulent or laminar. For the wings and tail surfaces, laminar flow is assumed for 10%, for the fuselage a value of 5% is assumed and for the nacelles a value of 2% is taken (30) .

14.5 Form Factor

The form factor term accounts for pressure drag caused by flow separation . Equation (17.8) gives the equation for form factor of the wings and tail surfaces, while equations (17.9) and (17.10) give the form factor for the fuselage and nacelles.

$$FF = \left(1 + \frac{0.6}{x_t}\left(\frac{t}{c}\right) + 100\left(\frac{t}{c}\right)^4\right)(1.34M^{0.18}(\cos\Lambda_m)^{0.28}) \tag{17.8}$$

$$FF_F = 1 + \frac{60}{(l_f/l_f)} + \frac{(l_f/l_f)}{400} \quad (17.9)$$

$$FF_N = 1 + \frac{0.35}{(l_N/l_N)} \quad (17.10)$$

14.6 Interference Factor

The interference factor accounts for mutual interference between components. The wing interference value chosen of 1 assumes an aerodynamically optimized wing-fuselage fairing. This is deemed appropriate as the upfront costs of development and the slight increase in weight are more than made up for in the significant reduction in drag especially for a commercial aircraft in high use. It is also appropriate to other A specific Q value for a T-tail is not given by literature however as the horizontal tailplane is continuous and therefore less affected by the fuselage, an optimistic value of 1.035 was selected as it is between the v-tail and conventional configuration. As this design's engines are fuselage mounted a value of 1.5 is selected for the nacelles while the fuselage has an interference factor of 1 as the interference factor is defined as the interference of components with the fuselage.

14.7 Miscellaneous, Leakage and Provenance Drag

The other major contribution to zero lift drag is the drag contribution of many smaller miscellaneous sources. The drag contribution of these sources is calculated in terms of (D/q) which is the drag area. The drag coefficient is then calculated by diving (D/q) by the reference area. The first source of additional drag is caused by the upsweep of the rear section of the fuselage. This causes flow separation and is described by equation (17.11) where u is the upsweep angle. Any rearward facing area, known as a base result in base drag as separation will occur. Base drag is given by equation (17.12) (for subsonic aircraft). The dimension of the base is dependent on the exhaust nozzle area of the APU.

$$\left(\frac{D}{q}\right)_{upsweep} = 3.83u^{2.5}A_{max} \quad (17.11)$$

$$\left(\frac{D}{q}\right)_{base} = (0.139 + 0.419(M - 0.161)^2)A_{base} \quad (17.12)$$

Along with roll control, spoilers also aid in reducing landing distance by intentionally increasing drag during landing. The drag area (D/q) of the spoilers is given by a constant 1.6 multiplied by the frontal area. The frontal area was found using the already determined span and length as well as by assuming a 48° deflection angle based on similar aircraft (31) For the undercarriage drag, the idea was to sum the CD_π for all undercarriage components (6). Knowing the dimensions of the undercarriages it is possible to know the drag they generate. Finally, it is possible to find the Cd for the undercarriage by using the reference surface

$$CD_\pi = \frac{D/q}{Frontal\ Aera} \quad (17.13)$$

$$CD = \frac{\sum_{Components} CD_\pi * Frontal\ Aera_{Components}}{S_{ref}} \quad (17.14)$$

To take everything into account, the initial value found must be multiplied by 1.2 to take into account the drag induced by the undercarriage doors that were left open. Furthermore, 7% more drag has to be added because the undercarriages are retractable. Finally, $CD_{U/C} = 0.006$. Losses due to the flow of air into and out of areas of low and high-pressure causing separation is known as leakage drag while protuberances consist of components which break up the previously assumed clean surface of the aircraft. The effect of these two sources combined is taken to contribute 3.5% of the total parasitic drag for a jet transport . Summing all terms in 17. Equation 17.2 gives the total zero lift drag for each flight segment was calculated as seen in table 17-2.

Take-off	W-C Cruise	C-H Cruise	H-W Cruise	Loiter	Cruise Missed approach	Landing*
0.0906	0.0284	0.0288	0.0289	0.0273	0.0291	0.1887

*Table 17-2 Total Zero lift drag for all mission segments *- With spoilers activated*

14.8 Wave Drag

Earlier in the design, the wings were swept such that the flow perpendicular to the wing was equal to the aerofoil's drag divergence Mach number. The drag divergence Mach number was defined as the Mach number at which there is a wave

drag of 0.002 however as the sweeping of the wing was determined based on the highest cruise Mach number, the other cruise segments will have different values for wave drag. To calculate the wave drag, an estimation for critical Mach number as being $(\frac{0.1}{80})^{1/3}$ (32) less than the drag divergence Mach number, is taken. Equation 17.15 (32) was then used to calculate the wave drag for cruise segments as can be seen in table 17.3. If $M<M_{DD}$, wave drag was taken to be zero.

$$C_{D,wave} = 20(M - M_{crit})^4 \tag{17.15}$$

As can be seen in table, the maximum Mach number cruise has a wave drag of 0.0023. This is close to the assumed value of 0.002 therefore validating the accuracy of all of the results.

Take-off	W-C Cruise	C-H Cruise	H-W Cruise	Loiter	Cruise Missed approach	Landing
0.0000	0.0008	0.0015	0.0018	0.0000	0.0023	0.0000

Table 17-3 Wave drag value for all mission segments s

14.9 Induced Drag

The total induced drag of an aircraft consists of the drag due to lift of the wing and horizontal tailplane and is given by equation (17.16)

$$C_{D_i} = \frac{{C_{l_w}}^2}{\pi A_{w,e} e_w} + \eta_H \left(\frac{S_H}{S_{ref}}\right) \frac{{C_l}^2{}_H}{\pi A_H e_H} \tag{17.16}$$

There are multiple methodologies to find the Oswald efficiency factor, equations (17.17) and (17.18) give a estimation for swept and upswept wings which is based on historical data which should therefore incorporate interference between the fuselage and wing as well as the induced drag of the fuselage. Interpolating between the two equations according to the sweep angle gives an expected conservative value of approximately 0.74 These factors however do not need to be accounted for again in the horizontal tailplane, therefore the method given by the equation by Howe (7) in appendix k provides a more appropriate idealized value of approximately 0.81-0.83.

$$e_{unswept} = 1.78\left(1 - 0.045{A_e}^{0.68}\right) - 0.64 \tag{17.17}$$

$$e_{swept} = 4.61(1 - 0.0045A^{0.68})\,(\cos\Lambda_{LE})^{0.15} - 3.1 \tag{17.18}$$

The value for C_{l_H} is calculated using equation (18.6) later in section 17.3 as it is dependent on stability concerns, specifically horizontal tail setting angle. Values for induced drag were then calculated as seen in table 17-4.

$$C_l = C_{l_w} + \eta_H \left(\frac{S_H}{S_{ref}}\right) C_{l_w} \tag{17.19}$$

The increase in induced drag at take-off and landing due to the deflection of flaps is given by equation 17.2 (6) where k_f is taken to be 0.28 as flaps are only partial span. Only a portion of the span having flaps results higher induced drag compared to full span flaps as partial span flaps disrupt the spanwise lift distribution. Adding the change in induced drag gives the total induced drag for all mission segments in table 17-4.

$$\Delta C_{D_i} = \left(\Delta C_{l_{flap}}\right)^2 \cos\Lambda_{25} \tag{17.20}$$

Take-off	W-C Cruise	C-H Cruise	H-W Cruise	Loiter	Cruise Missed approach	Landing
0.06785	0.00578	0.00578	0.00578	0.00578	0.00578	0.17967

Table 14-4 Total induced drag for all mission segments

14.10 Total Drag

Table 17-5 shows a summary of the three major components of drag as well as the summed total drag for all segments.

Take-off	W-C Cruise	C-H Cruise	H-W Cruise	Loiter	Cruise Missed approach	Landing*
0.1584	0.0349	0.0360	0.0366	0.0330	0.0372	0.3684

Table 14-5 Total induced drag for all mission segments

15 Stability

15.1 Longitudinal Static Stability

The main concern of longitudinal stability is the case of a sudden change in angle of attack, the aircraft should create a restoring moment that causes a pitch back to the free stream. In order to create this restoring pitching moment (C_{m_α}) we require that $\frac{\partial C_M}{\partial \alpha} < 0$. An expression for the moment acting around the centre of gravity is given in equation 18.1

$$\frac{\partial C_M}{\partial \alpha} = C_{L_\alpha w}\frac{(x_{ac,w} - x_{cg})}{\bar{c}} + C_{M_{\alpha f}} - \eta_H C_{L_\alpha h}\left(1 - \frac{\partial \varepsilon}{\partial \alpha}\right)\left(\frac{S_H}{S_w}\right)\frac{(x_{ac,h} - x_{cg})}{\bar{c}} \qquad (18.1)$$

Quantities such as the mean aerodynamic chord, the tail efficiency factor (η_H) and the lift curve slopes of the wing and horizontal stabilizer have been calculated in previous sections. $C_{M_{\alpha f}}$ is the pitching moment created by the fuselage and is given in equation (18.2) where factor K_f is found from the graph in appendix G according to statistical data.

$$C_{M_{\alpha f}} = K_f \frac{l_f {w_f}^2}{\bar{c} S_w} \qquad (18.2)$$

The downwash derivative $\frac{\partial \varepsilon}{\partial \alpha}$ accounts for how the flow about the horizontal stabilizer is affected by the angle of attack of the wings and is calculated using factors K_A, K_λ and K_h which relate the wing aspect ratio, sweep and the proximity of the tailplane and the wings to the downwash derivative. All these parameters were calculated as can be seen in the screenshot of the full stability calculations in Appendix H

These parameters were used in the equation (18.3) for the aircraft's power off neutral point which is the centre of gravity position for which $C_{m_\alpha} = 0$ when thrust effects are not accounted for, this means any c.g. point further aft of this will be unstable. The static margin of the aircraft can be found by taking the position of the c.g away from the neutral point position. To calculate the power on static margin the method following slides (2) was taken by increasing the static margin value by 2%. The upper limit was taken due to the large thrust our engines produce.

$$\frac{x_{np}}{\bar{c}} = \frac{C_{L_\alpha w}\frac{x_{ac\,w}}{\bar{c}} - C_{M_{\alpha\,f}} + \eta_h C_{L_\alpha h}\left(1 - \frac{d\varepsilon}{d\alpha}\right)\frac{S_h}{S_w}\frac{x_{ac\,h}}{\bar{c}}}{C_{L_\alpha w} + \eta_h C_{L_\alpha h}\left(1 - \frac{d\varepsilon}{d\alpha}\right)\frac{S_h}{S_w}} \qquad (18.3)$$

This must always be positive for a stable aircraft and shows the magnitude of the aircraft's stability. These static margins were calculated using the previous c.g. for weight and balance at three points take off at take-off landing and our average cruise segment and iterating though different placements of the wings and undercarriage to achieve static margins within a reasonable range for all the fight conditions. The furthest aft c.g. position is during take-off at MTOW. The static margin was made as small as possible while being stable at this point so that as the c.g. moves forward during the flight our aircraft is not too stable. This means smaller horizontal tailplanes can be used which is especially important as our fuselage mounted engines will increase the required size of the tailplanes.

Flight Condition	Neutral point(/c)	Centre of gravity (/c)	Power off static margin (/c)	Power on static margin (/c)
Cruise	4.5179	4.4647	0.0532	0.0732

Take-off	4.5407	4.4984	0.0422	0.0622
Landing	4.5223	4.3627	0.1596	0.1796

Table 18-1 Neutral point and Power on and Power off static margins for all flight phases

The static margin values for cruise and take-off are around the range of 4-7% that are typical for transport jet aircraft given in the slides (2) and all static margin values are less than the 20% maximum suggested hence the static margins were judged to be acceptable.

15.2 Directional Static Stability

The directional stability is determined by the moment derivative C_{N_β} being positive such that a change in direction of the flow laterally yaws the aircraft in that direction. The vertical tailplane provides a positive, stabilising contribution to the C_{N_β} derivative. As the β increases the vertical tail plane becomes a lifting surface and turns the aircraft into the flow. This must be large enough to counteract the destabilising effect the fuselage has on C_{N_β} so the vertical stabiliser has been sized using historical data of tail volume coefficients V_v to ensure it can provide directional stability.

15.3 Trim analysis

Once the stability of the aircraft due to longitudinal perturbations had been investigated a trim analysis of the aircraft was conducted to ensure steady level flight could be achieved throughout the aircraft's operational envelope. The moment arms about the centre of gravity of the thrust, wing and horizontal stabiliser could be used in equation (18.4) to calculate to total moment coefficient of the aircraft about the centre of gravity.

$$C_{Mcg} = -C_{Lw}\frac{(x_{ac\,w} - x_{cg})}{\bar{c}} + C_{M_0 w} + C_{M_{\alpha f}}\alpha - \eta_h C_{Lh}\frac{S_h}{S_w}\frac{(x_{ac\,h} - x_{cg})}{\bar{c}} + \frac{Z_t T}{qS_w\bar{c}} \tag{18.4}$$

The lift coefficients for the wing and tailplane were calculated using the lift curve slopes of the tail plane and wing and the corresponding angle of attack of each component accounting for downwash were relevant as seen in the equations 18.5 and 18.6 below

$$C_{Lw} = C_{L_{\alpha w}}(\alpha + i_w - \alpha_{ow}) \tag{18.5}$$

$$C_{Lh} = C_{L_{\alpha h}}\left[\alpha + i_w - \alpha_{ow}\left(1 - \frac{d\varepsilon}{d\alpha}\right) + (i_h - i_w) - (a_{oh} - \alpha_{ow})\right] \tag{18.6}$$

In this equation the setting of the elevator deflection had to be accounted for. This was done using a method specified in Raymer (6) where the elevator is treated as a plain flap with the deflection changing the zero-lift angle of attack only. The equations are provided below

$$\Delta\alpha_{0L} = -\frac{1}{C_{L_\alpha}}\frac{\partial C_L}{\partial \delta_f}\delta_f \tag{18.7}$$

$$\frac{1}{C_{L_\alpha}}\frac{\partial C_L}{\partial \delta_f} = 1.576\left({}^{C_f}/_{C}\right)^3 - 3.458\left({}^{C_f}/_{C}\right)^2 + 2.882\left({}^{C_f}/_{C}\right)$$

Where ${}^{C_f}/_{C}$ is the flap or elevator chord over the total tailplane chord. The zero lift moments were found using experimental data from our aerofoil for an unflapped aerofoil and flapped aerofoil in (33) then adjusted for the sweep and twist using the equation in the lecture notes (2). Where ${}^{C_f}/_{C}$ is the flap or elevator chord over the total tailplane chord. The zero lift moments were found using experimental data from our aerofoil for an unflapped aerofoil and flapped aerofoil in (33) then adjusted for the sweep and twist using the equation in the lecture notes (2). Now that all the values for equation 18.4 for the moment coefficient around the c.g. are known the incidence angle of the whole aircraft and the setting angle of the horizontal tailplane could be iterated. Trim plots shown in Appendix L, were made and the incidence and setting angle for trim at cruise could be extracted. As the horizontal tailplane is not adjustable the setting angle was set for cruise with no elevator deflection to reduce the lift induced drag of the tailplane this setting angle was then fixed

for all other flight conditions. The lift curve slope, zero lift angles of attack and design Cl were adjusted for take-off and landing and the same iteration was repeated but now deflecting the elevator instead. The angle of incidence and setting angle or elevator needed to achieve trim could then be obtained for take-off and landing conditions these are given in the table below. These values seem reasonable as the horizontal tailplane and elevator do not deflect excessively increasing the lift induced drag they would generate. They also do not dump any lift which means the wing does not have to generate extra lift to counteract a downforce at the tailplane.

Flight Condition	Design Cl	Moment Coefficient	Incidence angle(°)	Tailplane angle(°)	Elevator deflection(°)
Take-Off	2.400	0.0000	12.86	0.592	4.067
Cruise	0.363	0.0000	0.493	0.592	0.000
Landing	3.000	0.0000	15.78	0.592	0.498

Table 18-2 Aircraft incidence, tailplane setting angle and elevator deflection required for trim

16 Performance

16.1 Take-Off Distance

The take-off distance is calculated as the sum of 4 values which are: ground roll distance, rotation distance, transition distance and climb distance.

After applying the 15% safety factor in accordance with FAR25 regulations, we obtain:

$$S_{TO} = 1.15(S_G + S_R + S_{CL} + S_{TR}) \tag{19.1}$$

16.1.1 Ground Roll Distance

The distance is calculated using a purely physical law given below.

$$S_G = \frac{1}{2gK_A} \ln\left(\frac{K_T + K_A V_{LOF}^2}{K_T}\right) \tag{19.2}$$

Where:

$$K_T = \frac{T}{W} - \mu \tag{19.3}$$

$$K_A = \frac{\rho}{2(W/S)}\left(\mu C_L - C_{D_0} - \frac{C_L^2}{\pi\, AR\, e}\right) \tag{19.4}$$

μ is equals to 0.03 on dry runway and 0.05 on wet runway (brakes off). (6)

16.1.2 Rotation Distance

The rotation distance is given by the time taken to rotate to the liftoff attitude. For this size of aircraft, the time of rotation is assumed to be 3 seconds.

$$S_R = t_R V_{LOF} \tag{19.5}$$

16.1.3 Transition Distance and Climb Distance

The next equation relates the manoeuvre radius to the velocity during the transition and the load factor ($n = 1.2$ at take-off).

$$R = \frac{V_{TR}^2}{(n-1)g} \tag{19.6}$$

Knowing that $V_{TR} = 1.15V_{S,\,to}$ and that $V_{S,\,to}$ is directly linked to $C_{L_{max,\,t-o}} = 2.41$, the radius could be calculated $R = 2088m$. Concerning the angle of climb, the following equation has been used:

$$\gamma_{CL} \approx \sin^{-1}\left(\frac{T}{W} - \frac{1}{\frac{L}{D}}\right) \tag{19.7}$$

Where $\frac{T}{W} = 0.30$ and $\frac{L}{D} = 15.1$. The vertical distance travelled follows from it:

$$h_{TR} = R(1 - cos\gamma_{CL}) \tag{19.8}$$

Since $h_{OBS}(35\,ft) < h_{TR}$ the geometry gives:

$$S_{TR} = \sqrt{R^2 - (R - h_{OBS})^2} \tag{19.9}$$

$$S_{CL} = 0 \tag{19.10}$$

16.1.4 Take-off Distance Summary

	Distance on dry runway (m)	**Distance on wet runway (m)**
Ground Roll Distance $\boldsymbol{S_G}$	1112	1185
Rotation Distance $\boldsymbol{S_R}$	184	184
Transition Distance $\boldsymbol{S_{TR}}$	211	211
Climb Distance $\boldsymbol{S_{CL}}$	0	0
Total Take-Off Distance $\boldsymbol{S_{TO}}$ (includes 15% security factor)	**1733**	**1816**

Table 16-1 Take-off Distance Summary

In all cases the total take-off distance is lower than the minimum take-off distance available (2119m).

16.2 Balanced Field Length

To ensure safe take-off in the event of an engine loss, the calculation of the balanced field length is essential. The equation used is semi-empirical:

$$BFL = \frac{0.863}{1 + 2.3G}\left(\frac{\frac{W}{S}}{\rho g C_{L_{climb}}} + h_{OBS}\right)\left(\frac{1}{\frac{\bar{T}}{W} - U} + 2.7\right) + \frac{655}{\sqrt{\sigma}} \tag{19.11}$$

Where:

$$G = \gamma_{CL} - \gamma_{min} \qquad \gamma_{CL} = sin^{-1}\left[0.5\left(\frac{T}{W}\right)_0 - \frac{D_{OEI}}{W_0}\right] \text{ evaluated at } V_{CL}$$

$$U = 0.01 C_{L_{max\,clean}} + 0.02 \qquad \gamma_{min} = 0.024 \quad \text{(2 engines)}$$

And the mean thrust produced by a turbofan during take-off is:

$$\bar{T} = 0.75 T_0\left(\frac{5 + BPR}{4 + BPR}\right) \tag{19.12}$$

The drag D_{OEI} with only one engine operative is calculated using these equations ($L = W$ at V_{CL}):

$$\frac{D_{OEI}}{W} = \frac{D_{AOE} + \widetilde{D}}{W} = \frac{D_{AOE}}{L} + \frac{\widetilde{D}}{W} \tag{19.13}$$

Where $\widetilde{D}$ is the drag inducted by the inoperative engine (6):

$$\widetilde{D} = 0.3(0.5\rho_0 V_{LOF}^2)(\pi R_{engine}^2) \tag{19.14}$$

An important verification is to ensure that the balanced field length is less than the take-off distance available.

BPR	$\boldsymbol{R_{engine}}$ (m)	$\boldsymbol{D_{AOE}/L}$	$\boldsymbol{D_{OEI}/W}$	$\boldsymbol{\gamma_{CL}}$ (rad)	**BFL (m)**
5.4	0.903	0.0662	0.00391	0.046	**802**

Table 19-2 Summary of main values for balanced field length calculation

16.3 Landing Distance

Like for the take-off distance calculation, the landing distance is the sum of 4 distances: the approach distance, the flare distance, the touchdown distance and the braking distance. In compliance with FAR25 regulations, a security factor of 1.666 is applied:

$$S_L = 1.666(S_a + S_F + S_{FR} + S_B) \quad (19.15)$$

16.3.1 Approach Distance

The approach segment represents the ground covered while descending from h_{OBS} to the flare height (h_F).

$$S_a = \frac{h_{OBS} - h_F}{\tan \gamma_a} \quad (19.16)$$

Where $\gamma_a = 3\ deg$ is the descent gradient. The flare height is found thanks to the flare radius:

$$h_F = R(1 - \cos \gamma_a) \quad (19.17)$$

Where $R = \frac{V_F^2}{(n-1)g}$ and $V_F \approx 1.23 V_S$.

16.3.2 Flare Distance and Touchdown Distance

The distance covered during the flare is given by the geometry:

$$S_F = R \sin \gamma_a \quad (19.18)$$

After the touchdown the aircraft will not be able to use reverse thrust or breaks for few seconds. The distance travelled is then:

$$S_{FR} = t_{FR} V_{TD} \quad (19.19)$$

Where $V_{TD} \approx 1.15 V_S$ and t_{FR} = 1-3 s. To evaluate the aircraft performance under worst conditions t_{FR} has been chosen to be 3s.

16.3.3 Braking Distance

Like for the ground roll distance during the take-off, the braking distance is calculated thanks to a physical equation:

$$S_B = \frac{1}{2gK_A} \ln\left(\frac{K_T + K_A V_2^2}{K_T + K_A V_1^2}\right) \quad (19.20)$$

Expressions for K_T and K_A can be found in the paragraph 17.1.1. The braking manoeuvre is done in 2 steps:

- Full breaks as well as the thrust reversers are used while the velocity is greater than 50 kts.
  During this period:
  $$\begin{cases} \frac{T_{rev}}{W} = -0.4\left(\frac{T}{W}\right)_0 \\ V_2 = 50\,kts = 25.7\,m/s \\ V_1 = V_{TD} \end{cases}$$

- Under 50 kts and until full stop, thrust reverses are no longer used due to safety reasons. (2)
  During this period:
  $$\begin{cases} \frac{T_{idle}}{W} = 0.15\left(\frac{T}{W}\right)_0 \\ V_2 = 0 \\ V_1 = 50\,kts = 25.7\,m/s \end{cases}$$

The use of spoilers leads to a $C_L \approx 0$ and an increase in $C_{D_0} = 0.1887$.

16.3.4 Landing Distance Summary

	Distance (m) on dry runway ($\mu = 0.5$(6))	Distance (m) on wet runway ($\mu = 0.3$(6))
With thrust reversers	$S_a = 154$ $S_F = 100$ $S_{FR} = 172$ $S_B = 273$ $\boldsymbol{S_L = 1164}$	$S_a = 154$ $S_F = 100$ $S_{FR} = 172$ $S_B = 414$ $\boldsymbol{S_L = 1400}$
Without thrust reversers	$S_a = 154$ $S_F = 100$ $S_{FR} = 172$ $S_B = 331$ $\boldsymbol{S_L = 1261}$	$S_a = 154$ $S_F = 100$ $S_{FR} = 172$ $S_B = 552$ $\boldsymbol{S_L = 1628}$

Table 19-3 Summary of Landing Distance values considering dry and wet runway

In all cases the total landing distance is lower than the minimum landing distance available (1815m).

16.4 Mission performance

The main performance the aircraft should have is its capability to operate the mission profile.

To do so, all weight fractions used during the initial sizing are assumed to be the same (warm-up, taxi, take-off, climb, descent and landing). Idling and diversion segment weight fractions have been calculated thanks to the updated SFC and engine thrust values. The maximum cruise range is determined with the following equations:

$$\frac{W_n}{W_0} = \frac{W_0 - W_{fuel}}{W_0} = \prod_{j \neq cruise} \frac{W_j}{W_{j-1}} \prod_{j=cruis} \frac{W_j}{W_{j-1}} \qquad \xrightarrow{yields} \prod_{j=cruis} \frac{W_j}{W_{j-1}} = \frac{\frac{W_0 - W_{fuel}}{W_0}}{\prod_{j \neq cruise} \frac{W_j}{W_{j-1}}} \qquad (19.21)$$

The product of $\frac{W_j}{W_{j-1}}$ considers all 2 idling, warm-up, 3 taxi, 3 take-off, 3 climb, 3 descent, 3 landing and diversion segments. The maximum cruise range is then:

$$R_{max} = -\frac{V_{cruise}\left(\frac{L}{D}\right)_{cruise}}{SFC} \ln\left(\prod_{j=cruise} \frac{W_j}{W_{j-1}}\right) \qquad (19.22)$$

An analysis of the aircraft range can therefore be done since the aircraft range can be increased by removing payload (cannot add fuel since the fuel tanks are already full).

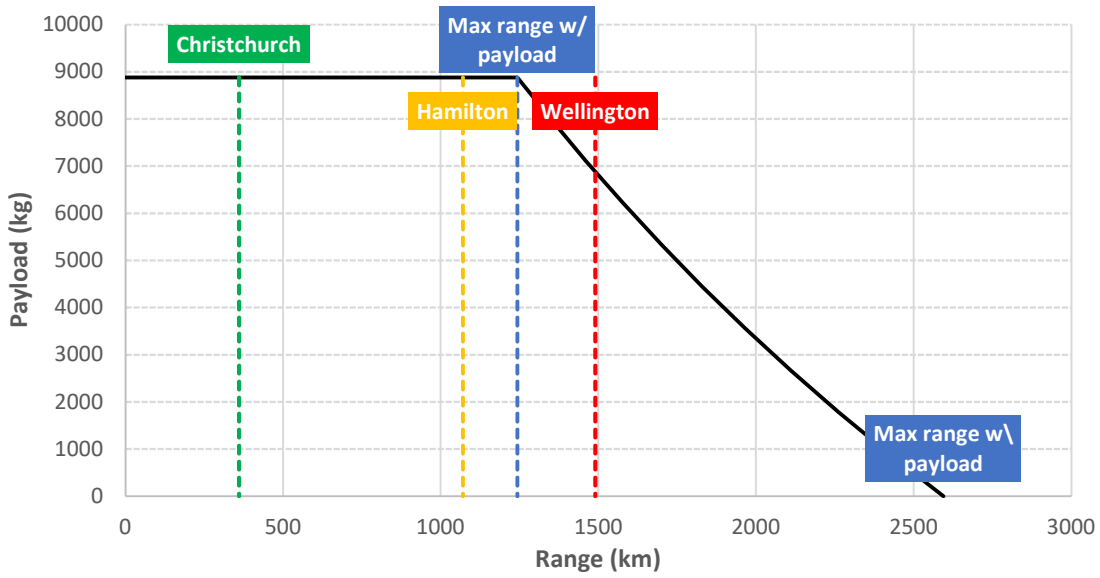

Figure 2 Aircraft range analysis

In the present case, the aircraft does not have enough fuel to travel all the mission profile segments. This is directly linked to the L/D value of 10.05 during cruise while it was estimated at 13.86 during the initial sizing of the aircraft. At this stage, 658 kg of fuel are missing to complete all legs.

16.5 Flight Envelope

The flight envelope can be analysed thanks to the plot of the specific excess power. It is a way to quickly identify the required Mach at a given altitude in order to achieve a wanted vertical speed value. In particular, the plot is useful to find the absolute and service ceilings as well as the maximum Mach number achievable by the aircraft. The specific excess power P_S is obtained by calculate the thrust and the drag at a specific velocity and altitude:

$$P_S = V\left(\frac{T-D}{W}\right) \tag{19.23}$$

While the density and the temperature are determined by using standard atmosphere equations (32), the thrust is a function of the velocity and altitude (2):

$$\left(\frac{T}{W}\right)_0 = \frac{\alpha}{\beta}\left[\frac{1}{V}V_v + \frac{\frac{1}{2}\rho V^2 C_{D_0}}{\alpha\, W/S} + \frac{\alpha n^2 W/S}{\frac{1}{2}\rho V^2 \pi\, AR\, e}\right] \tag{19.24}$$

V_v is the vertical velocity, $\alpha = \frac{W}{W_0}$ is equals to 1 assuming the aircraft begins its mission and $\beta = \frac{T}{T_0}$ is determined by using Howe's method (16) ($M < 0.9$):

$$\beta = F[K_1 + K_2 BPR + (K_3 + K_4 BPR)M]\sigma^s \tag{19.25}$$

Where F is a factor in the case of an afterburner use which is not the case for this aircraft. K_1, K_2, K_3 and K_4 are constants depending on the bypass ratio and if the Mach is greater or lower than 0.4. Due to the lack of information above 11000m and considering our bypass ratio of 5.4, s is always equals to 0.7 while σ is equal to $\frac{\rho}{\rho_0}$ for an altitude lower than 11000m and is being constant above that $\sigma = \frac{\rho_{11000}}{\rho_0}$.

The drag is known by using the drag polar equation and add a wave drag effect after M_{crit}. Therefore, to plot the flight envelope, the problem amounts to search a velocity (directly linked to the Mach thanks to the sound speed) in such way that for a given altitude and vertical velocity:

$$V\left[\frac{T(V,h)}{W}-\frac{D(V,h)}{W}\right]-V_v=0 \qquad (19.26)$$

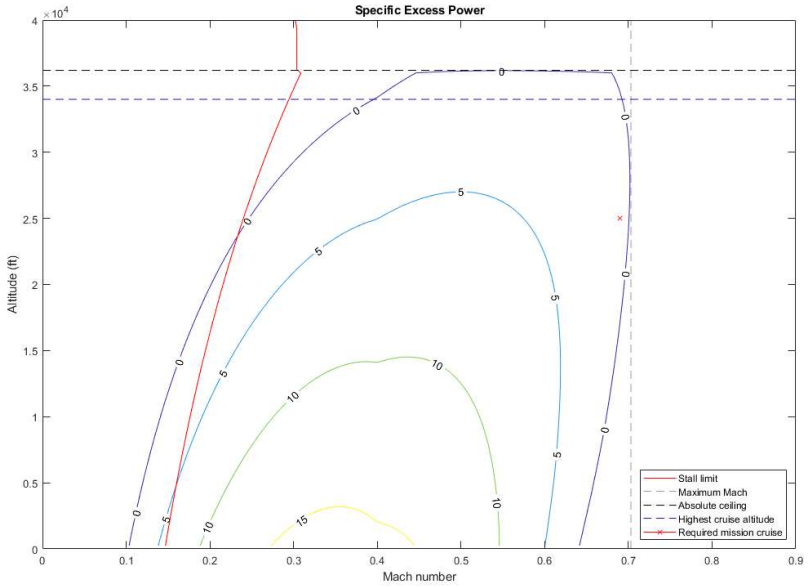

Figure 3 Specific Excess Power – Flight envelope plot. Curves represent vertical velocity in 1/100 ft/min

This plot shows that the aircraft can fly at 36200ft which is under the required absolute celling of 40000ft. This is also the case for the Mach number where the highest Mach achievable for the aircraft is calculated at 0.703, under the 0.75 required. It is important to note that the plot is extremely sensible to any thrustor drag changes. The Howe's method, containing approximations and discontinuities after 11000m, is part of the bad performance obtained. The aircraft suffers from too much drag compared to the initial sizing which combined with the incertitude about Howe's method leads to a lack of specific excess power.

17 Discussion

17.1 Conclusion and Improvements

In terms of performance the initial mission profile was not accomplished as seen in the flight envelope due to lower lift to drag ratio as well as a worst thrust than expected due to an increase of specific fuel consumption. However, the aircraft is successfully stable and was able to reach the fairly high estimations of maximum lift coefficient. The design is however, able to meet all landing and take-off constraints, including balance field length. Since the empty weight is lower than expected, further iterations focused on improving efficiency, specifically focused on drag and propulsion would likely result in the mission profile being completed successfully. Other possible improvements to this design could include.

- Possible change in design configuration. This would accommodate more efficient higher bypass ratio engines as well as decrease drag, and weight penalties associated with aft mounted engines and a T-empennage.
- Expanding aerofoils considered to super critical aerofoils which have higher drag divergent Mach numbers. This allows for a thicker aerofoil to be selected therefore reducing weight while still having low sweep.
- Reduction in vertical tail size. The actual lever arms were less than assumed for initial predictions resulting in significantly larger vertical tail than is optimal. Possible solutions would involve a thicker and therefore lighter wing, a longer fuselage, or a change in configuration from a aft mounted engine.
- Undercarriage to close of the last spar of the wing, resulting in a necessity of designing a more complex retraction system

18 References

1. Levis, Errikos. *Coursework Briefing Sheet.* London : Imperial College London, Department of Aeronautics, 2022-23.

2. —. *Aerospace Vehicle Design - Conceptual Design.* [Lecture Slides] London : Imperial College London, Department of Aeronautics, 2022-23.

3. Roskam, Jan. *Airplane Design Part I: Preliminary Sizing of Airplanes.* illustrated, reprint. s.l. : DARcorporation, 1985.

4. Kallstrom, Kristen. *Exploring Airfoil Table Generation using XFOIL and OVERFLOW.* Moffett Field : NASA, 2022.

5. Mason, W.H. Transonic Aerodynamics of Airfoils and Wings. [Online] 10 March 2006. https://archive.aoe.vt.edu/mason/Mason_f/ConfigAeroTransonics.pdf.

6. Raymer, Daniel P. *Aircraft Design : A Conceptual Approach.* Sixth edition. s.l. : American Institute of Aeronautics and Astronautics, 2018.

7. HOOU. *Aircraft design.*

8. FAA. Aeroynamics of Flight. [Online]

9. AirShaper. How do winglets improve aerodynamics? [Online] https://airshaper.com/videos/how-do-winglets-improve-aerodynamics/ubvr1w1hH80.

10. Maurizio Verrastro, Ignazio Dimino. Winglet. [Online]

11. Rudolph, Peter K.C. *High-Lift Systems on Commercial Subsonic Airliners.* s.l. : NASA, 1996.

12. European Union Aviation Safety Agency. *Type-Certificate: Data Sheet.* Cincinnati : EASA, 2020.

13. Teal Group Corporation. World Power Systems Briefing. [Online] 2022. [Cited: 02 12 2022.] http://tealgroup.com/images/TGCTOC/sample-babeng.pdf.

14. D.Rhodes, L.Jenkinson P.Simpkin. *Civil Jet Aircraft Design.* s.l. : Arnold Publishers, 1999.

15. Jackson, Paul. *Jane's All the World's Aircraft.* s.l. : Jane's Information Group, 2007.

16. Torenbeek, Egbert. *Synthesis of Subsonic Airplane Design.* s.l. : Kluwer Academic Publishers Group, 1982.

17. Nicolin, Ilie and Nicolin, Bogdan Adrian. *The fly-by-wire system.* Bucharest : INCAS - National Institute for Aerospace Research "Elie Carafoli", 2019.

18. Opencockpits. Stick Shaker. [Online] 2018. https://www.opencockpits.com/catalog/stick-shaker-p-587.html?language=en#:~:text=The%20Stick%20Shaker%20is%20a,Weight%3A0%2C610Kg.

19. CRJ Regional Jet. *CRJ900 Electrical System.*

20. Honeywell. RE220 Auxiliary Power Unit. *Aerospace Honeywell.* [Online] https://aerospace.honeywell.com/us/en/products-and-services/product/hardware-and-systems/auxiliary-power-units/re220-apu.

21. Airbus. *Airbus A220 Technical Training Manual - Electrical Bombardier CSeries CS300.* 2006.

22. Nurcombe, M. Dechow & C.A.H. *Air Quality in Airplane Cabins and Similar Enclosed Spaces.* 2005.

23. Tooren, Michel van and Krakers, Lars. *Multi-disciplinary Design of Aircraft Fuselage Structures* . s.l. : American Institute of Aeronautics and Astronautics , 2007.

24. Prasad, N. Eswara and Wanhill, R. J. H. Aluminium Alloys for Aerospace Applications. *Aerospace Materials and Material Technologies: Volume 1: Aerospace Materials.* 2017, pp. 29-52.

25. Ti-TEK Ltd. Titek Titanium Specialists. [Online] 2022. https://titek.co.uk/titanium-in-aerospace/#:~:text=As%20the%20aerospace%20industry%20emerged%20in%20the%201950s%2C,blades%2C%20pumps%20and%20screens%20within%20the%20aircraft%20engine..

26. The Goodyear Tire & Rubber Company. Good Year Aviation Tires. [Online] 2022. https://www.goodyearaviation.com/search/tire-results-mfg.html?search=product&mfg=Bombardier&model=CRJ900&position=&size=&partnumber=&market=&returnformat=json.

27. Yetter, J. A. *Why Do Airlines Want and Use Thrust Reversers? - A Compilation of Airline Industry Responses to a Survey Regarding the Use of Thrust Reversers on Commercial Transport Airplanes.* Hampton, Virginia : NASA, 1995.

28. Titanium vs Aluminum. *Titanium Processing Center.* [Online] https://www.titaniumprocessingcenter.com/titanium-vs-aluminum/.

29. Chai, S., Crisafulli, P. and Mason, W. H. *Aircraft Center of Gravity Estimation in Conceptual/Preliminary Design.* Blacksburg, Virginia : American Institute of Aeronautics and Astronautics, Inc., 1995.

30. *Aspects of aero-engine nacelle drag.* Robinson, Matthew, MacManus, David G. and Sheaf, Christopher. 5, s.l. : SAGE, 2018, Vol. 233.

31. Brady, Chris. The Boeing 737 Technical Site. [Online] 1999. http://www.b737.org.uk/flightcontrols.htm.

32. Diehl, Walter S. *Standard Atmosphere - Tables and Data.* s.l. : NASA, 1926.

33. Scholz, Dieter. Aircraft Design. [Online] 2015. http://hoou.ProfScholz.de .

34. Jennions, Ian and Ali, Fakhre. Simulation of an aircraft environmental control system. *Applied Thermal Engineering.* 25 May 2020.

35. Roskam, Jan. *Airplane Design Part II: Preliminary Configuration Design and Integration of the Propulsion System.* s.l. : DARcorporation, 1985.

36. Houghton, E. L., et al. *Aerodynamics for Engineering Students.* s.l. : Butterworth-Heinemann, 2015.

37. Kapania, Rakesh K., et al. *Multidisciplinary Design Optimization and Cruise Mach Number Study of Truss-Braced Wing Aircraft.* Blacksburg : NASA, 2018.

38. Radespiel, Rolf, Pfingsten, Kai Christoph and Jensch, C. *Flow Analysis of Augmented High-Lift Systems.* Braunschweig : TU Braunschweig, 2009.

39. Abbott, Ira H. and Von Doenhoff, A. E. *Theory of Wing Sections: Including a Summary of Airfoil Data.* New York : Dover Publications Inc., 1960.

40. Casinader, Trevin. Bombardier CRJ 900 Guide and Specs: All You Need to Know. *Aviator Insider.* [Online] Astra WordPress Theme, 2022. https://aviatorinsider.com/airplane-brands/bombardier-crj-900/.

19 Appendices

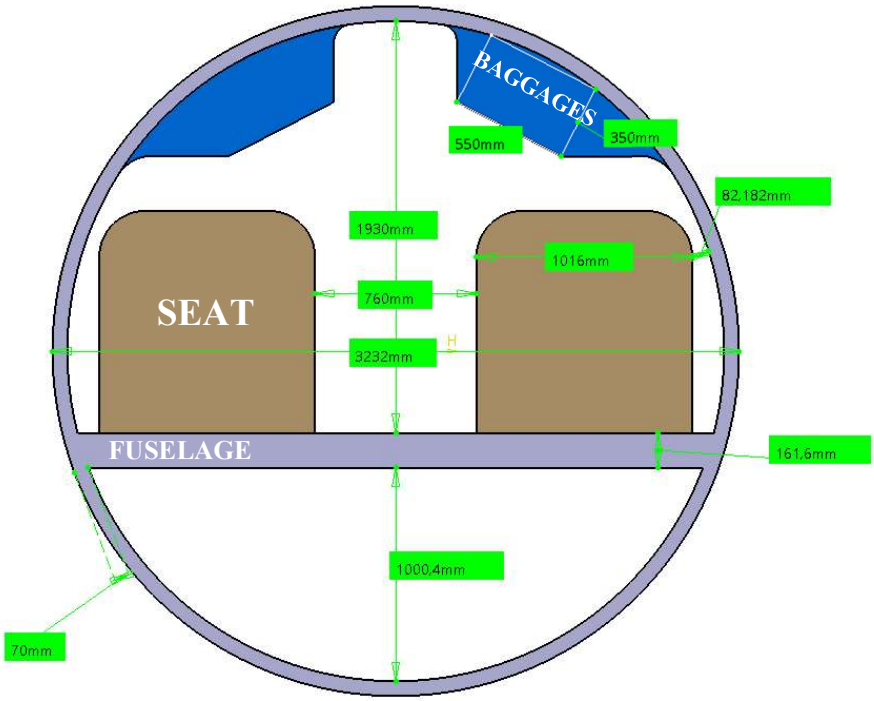

Appendix A - Cross Section

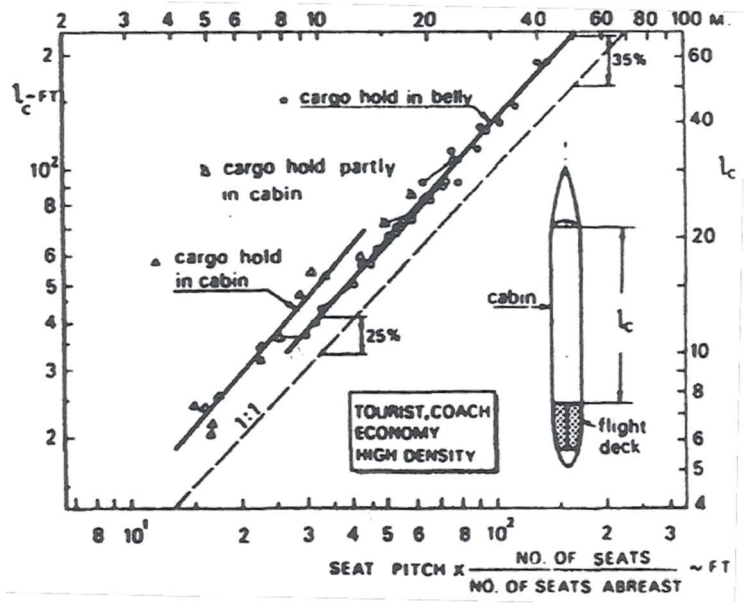

Appendix B - Empirical law to determine the length of the cabin [Torenbeek]

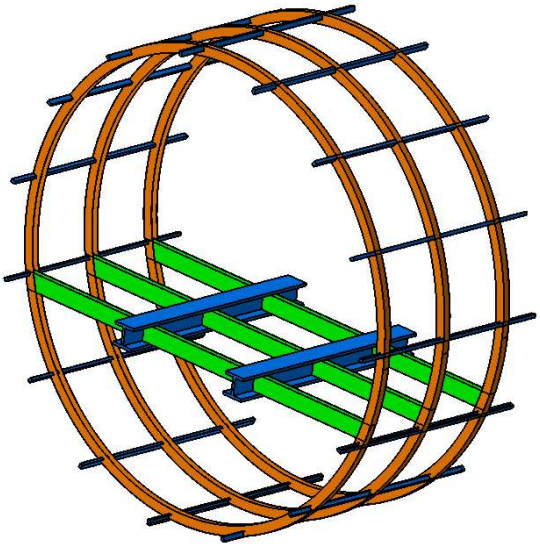

Appendix C - Simplified representation of the fuselage structure

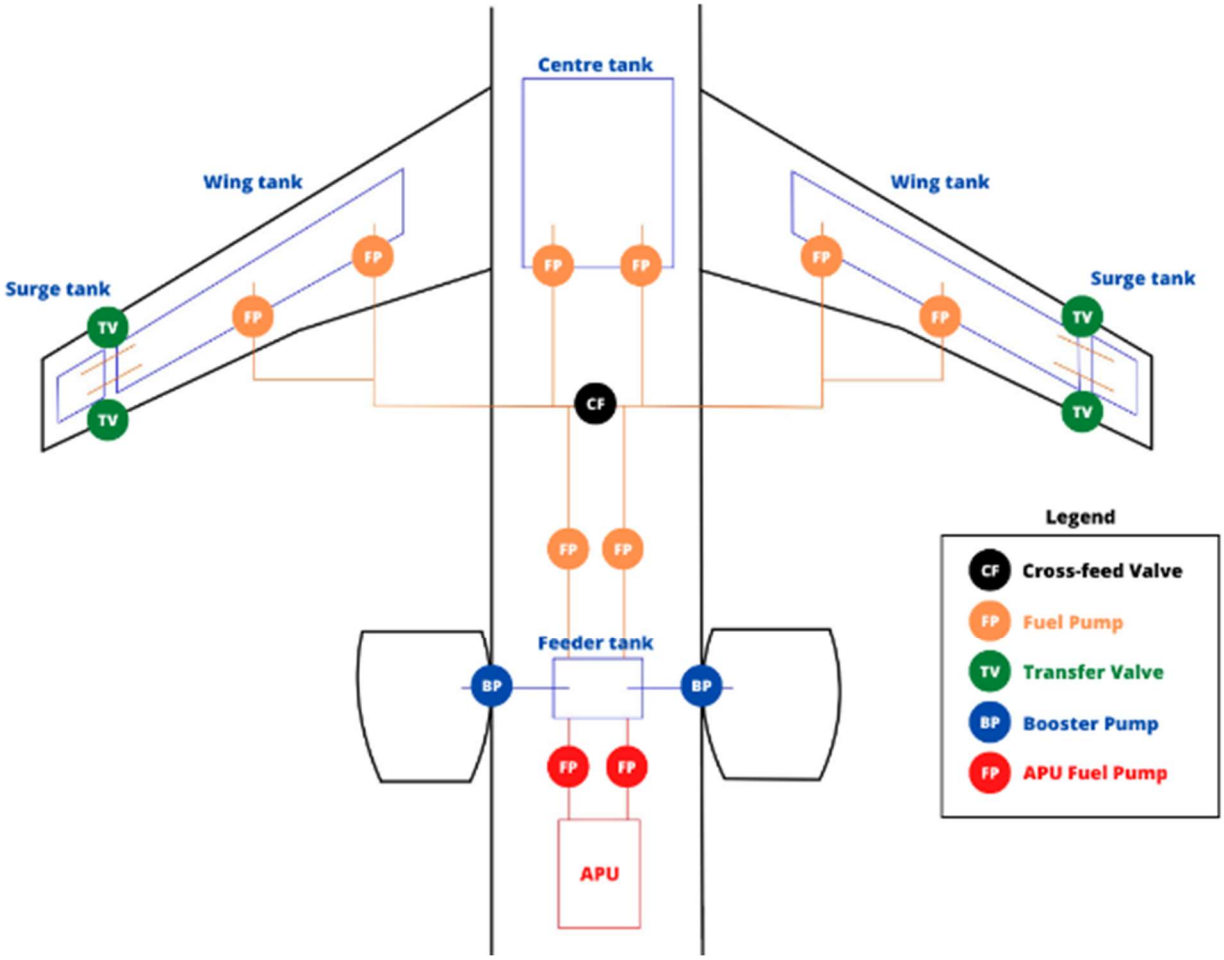

Appendix D

A

Table 19-1

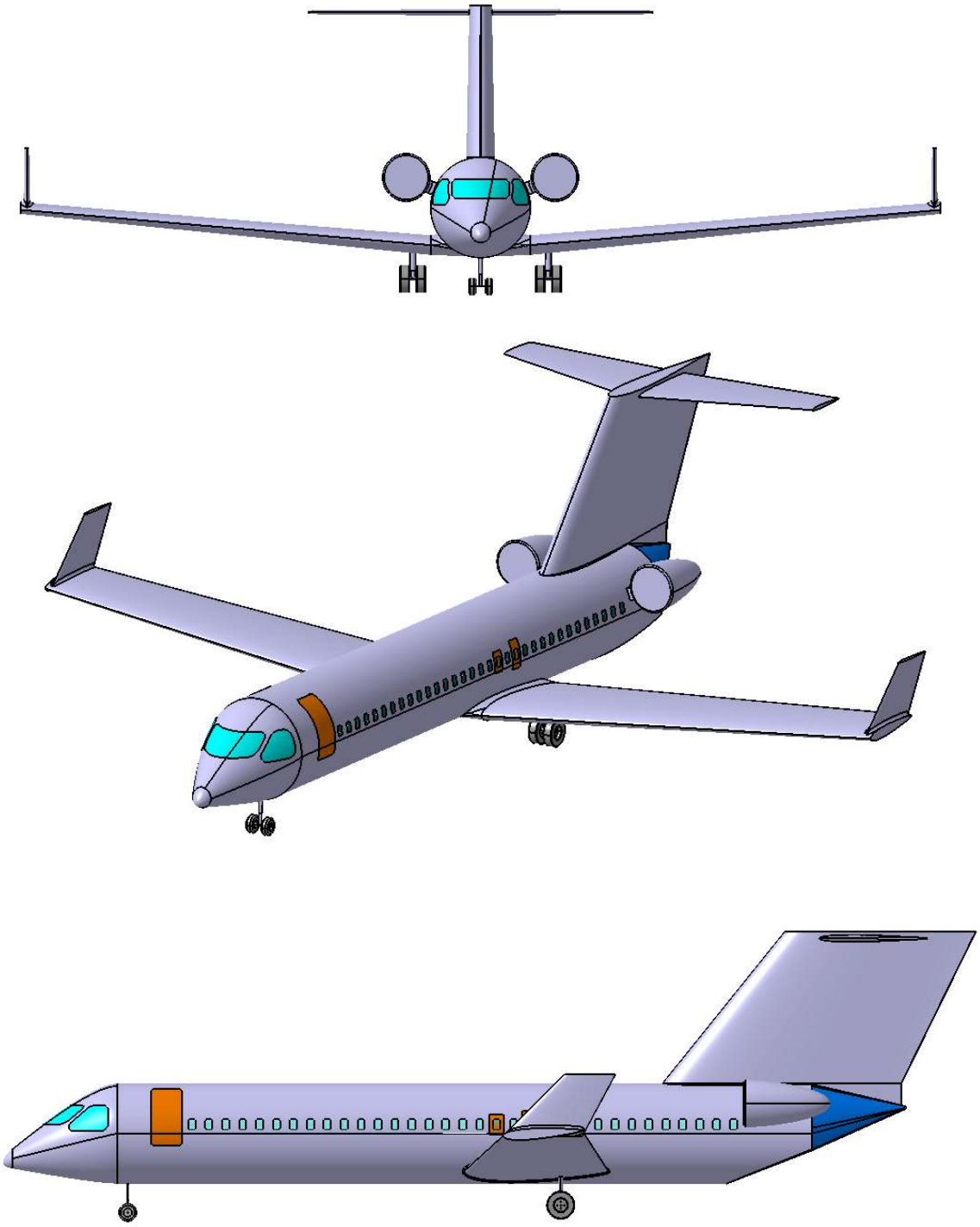

Appendix E Three View of the Aircraft

Table 19-2

weight of engine components (gear box, generator etc)	Weight (kg)
Oil pump	4.67
IDG(generator)	36.83
Air Turbine Starter	12.56
Hydralic Pump	4.34
Alternator	1.36
Fuel Pump	12.97
Total weight	72.73

Appendix F

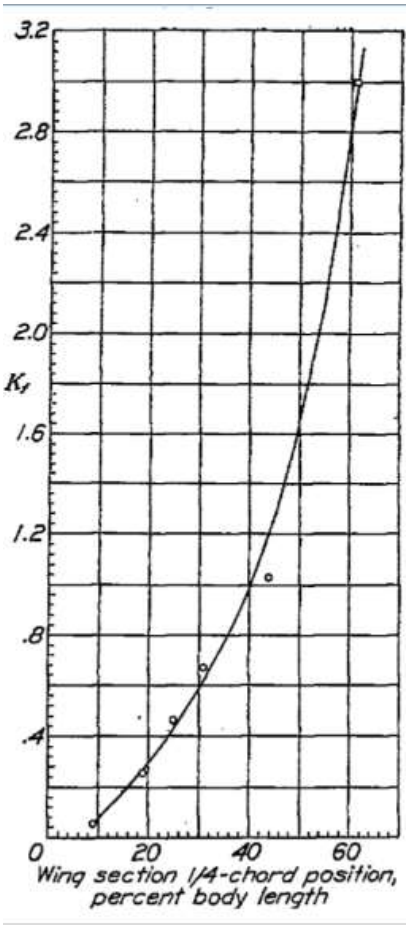

Appendix G

Wing Center of pressure		16.3179
cg (x)	16.371927	
cg (z)	0.0027255	
Engine Thrust arm(z)	0.96948	
Area of horizontal tail	28.635129	
Lift curve slope of wing (cruise)	6.34	8.0807
Mean aerodynamic chord	3.6669474	
nH	1	
Lift curve slope of horizontal tailplane	4.62034	
(1-downwash deriv)	0.7010675	
Ka	0.082411	
Klambda	1.2265791	
Kh	0.7682131	
Sweep	0.0578066	
hh	8.0911497	
horizontal lever arm	12.780754	29.0987
de/daoa	0.2989325	
Fuselage pitching moment coefficient		
Fuselage length	29.31	
Fuselage max width	3.2316	
K fuselage factor	3.1	
CM alpha f	2.4633512	
Xnp	4.5349884	

Appendix H

High lift device	$\Delta C_{l_{max}}$
Flaps	
Plain and split	0.9
Slotted	1.3
Fowler	$1.3\,c'/c$
Double slotted	$1.6\,c'/c$
Triple slotted	$1.9\,c'/c$
Leading edge devices	
Fixed slotted	0.2
Leading-edge flap	0.3
Kruger flap	0.3
Slat	$0.4\,c'/c$

Appendix I

$$S_{wet,N} = S_{wet,fan\ cowl.} + S_{wet,gas\ gen.} + S_{wet,plug} \tag{13.11}$$

$$S_{wet,fan\ cowl.} = l_n \cdot D_n \cdot \left[2 + 0.35\frac{l_1}{l_n} + 0.8 \cdot \frac{l_1 \cdot D_{hl}}{l_n \cdot D_n} + 1.15 \cdot \left(1 - \frac{l_1}{l_n}\right) \cdot \frac{D_{ef}}{D_n} \right] \tag{13.12}$$

$$S_{wet,gas\ gen.} = \pi \cdot l_g \cdot D_g \cdot \left[1 - \frac{1}{3} \cdot \left(1 - \frac{D_{eg}}{D_g}\right) \cdot \left(1 - 0.18 \cdot \left(\frac{D_g}{l_g}\right)^{\frac{5}{3}} \right) \right] \tag{13.13}$$

$$S_{wet,plug} = 0.7 \cdot \pi \cdot l_p \cdot D_p \tag{13.14}$$

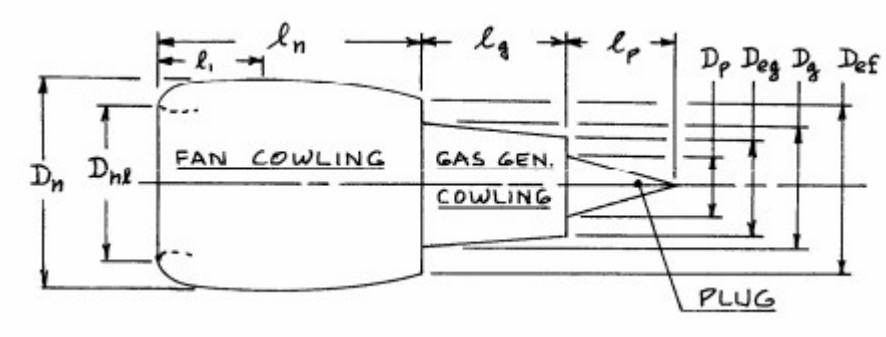

Appendix J

According to **Howe 2000** (equation 6.14a), the Oswald factor e can be estimated for the subsonic range and for transonic flows (M < 0.95) for aircraft with a wing aspect ratio of $A > 5$ from

$$e = \frac{1}{(1+0.12\,M^6)\left\{1+\dfrac{0.142+f(\lambda)\,A\,(10\,t/c)^{0.33}}{(\cos\varphi_{25})^2}+\dfrac{0.1\,(3\,N_e+1)}{(4+A)^{0.8}}\right\}} \quad . \qquad (13.26)$$

In this equation

M is the flight Mach number

A is the (effective) aspect ratio

t/c is the relative airfoil thickness

φ_{25} is the wing sweep of the 25% line

N_e is the number of engines **on** the wing (if none, then $N_e = 0$).

$$f(\lambda) = 0.005\left(1+1.5\,(\lambda-0.6)^2\right) \quad . \qquad (13.27)$$

Appendix k


Trim plot for cruise
0.02
0.01
0
-0.01
-0.02
-0.03
-0.04
-0.05
0.3
0.35
0.4
0.45
0.5
0.55
0.6
q
0.5
1
0.8
0.7
0.6
0.9
Cl design


Trim plot for take-off
0.02
0.01
0
-0.01
-0.02
-0.03
2
2.2
2.4
2.6
2.8
3
4.2
4.1
4
Cl design

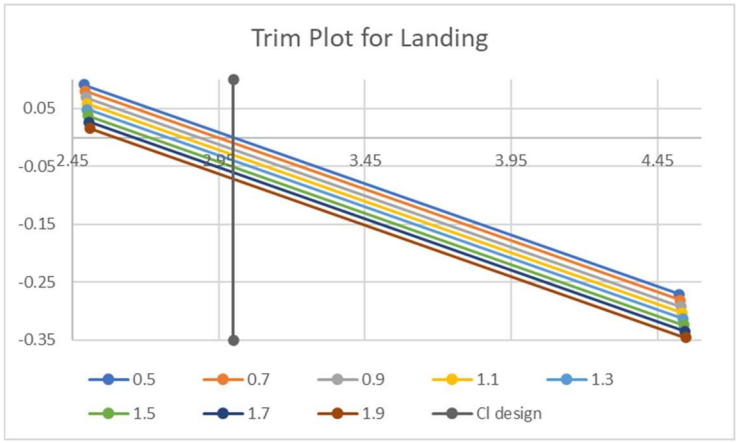
Trim Plot for Landing
0.05
-0.05
-0.15
-0.25
-0.35
2.45
3.45
3.95
4.45
0.5
0.7
0.9
1.1
1.3
1.5
1.7
1.9
Cl design

Appendix L